Distribution Agreement

In presenting this thesis as a partial fulfillment of the requirements for a degree from Emory University, I hereby grant to Emory University and its agents the non-exclusive license to archive, make accessible, and display my thesis in whole or in part in all forms of media, now or hereafter known, including display on the World Wide Web. I understand that I may select some access restrictions as part of the online submission of this thesis. I retain all ownership rights to the copyright of the thesis. I also retain the right to use in future works (such as articles or books) all or part of this thesis.

Lucas Alonso-Muñoyerro April 7, 2023

An analysis of Stellar Kinematics in a Sample of Quiescent Galaxies using the Galaxy IFU Spectroscopy Tool (GIST) and IFS data from the Atlas^{3D} Project.

By

Lucas Alonso-Muñoyerro

Merida Batiste, Ph.D.
Advisor

Physics and Astronomy

Merida Batiste, Ph.D.
Advisor

Alissa Sue Bans, Ph.D.
Committee Member

Adam Tahir Mirza, Ph.D.
Committee Member

2023

An analysis of Stellar Kinematics in a Sample of Quiescent Galaxies using the Galaxy IFU Spectroscopy Tool (GIST) and IFS data from the Atlas^{3D} Project.

By

Lucas Alonso-Muñoyerro

Merida Batiste, Ph.D.
Advisor

An abstract of
a thesis submitted to the Faculty of Emory College of Arts and Sciences
of Emory University in partial fulfillment
of the requirements for the degree of
Bachelors of Science with Honors

Physics and Astronomy

2023

Abstract

An analysis of Stellar Kinematics in a Sample of Quiescent Galaxies using the Galaxy IFU Spectroscopy Tool (GIST) and IFS data from the Atlas^{3D} Project.

By Lucas Alonso-Muñoyerro

In this project we extract the stellar kinematics for a sample of six quiescent galaxies within the Atlas^{3D} sample for which there is photometric evidence of structure. The analysis is done by means of pPXF and the GIST pipeline. In an effort to understand the intrinsic scatter of $\sigma_\star$ in the $M_\bullet - \sigma_\star$ relation, we perform an analysis on the effect of effective radius. We provide evidence on the overestimation of the effective radius by Cappellari et al. (2011) where it can be $5\times$ or $17\times$ overestimated depending on the morphology of the galaxy bulge and find that the choice of effective radius can have a considerable effect on the relation, explaining some of the scatter in $\sigma_\star$. We also provide a preliminary batch processing code as a first step towards a large-scale analysis of the SAURON-observed galaxies.

An analysis of Stellar Kinematics in a Sample of Quiescent Galaxies using the Galaxy IFU Spectroscopy Tool (GIST) and IFS data from the Atlas^{3D} Project.

By

Lucas Alonso-Muñoyerro

Merida Batiste, Ph.D.
Advisor

A thesis submitted to the Faculty of Emory College of Arts and Sciences
of Emory University in partial fulfillment
of the requirements of the degree of
Bachelor of Science with Honors

Physics and Astronomy

2023

Acknowledgments

I want to acknowledge first and foremost my advisor, Dr. Merida Batiste, for her interest and unconditional help in this project. Her constructive feedback and good mood, even when times were tough, were key in my analysis and writing process. She impressed upon me a passion for astrophysics and a deep understanding of research for which I will always be thankful for. I also would like to thank my family (i.e. mother, father, brothers) for showing me love at my most irritable moments, regardless of whether the thesis was being written or not. It is hard to have and to be a son and brother sometimes. This project would also have not been possible if it weren't for the great resources provided by Michelle, Eric, and Adrian. You will always have a place in my heart. Lastly, I want to thank my other two committee members, Dr. Alissa Bans and Dr. Adam Mirza for providing their support for and accepting to be a part of this project. I performed my first official observations (not just of the moon) alongside Dr. Bans, and I will never not get excited when witnessing the opening of a dome. Dr. Mirza is also a professor that I will always be thankful for. Although we didn't get to talk much about my project (absolutely my fault), in his classes I was able to discover a side of music I had never, but always wanted to explore. He pushed me to understand and embrace my creative power. Lastly, I want to thank my life companion, procrastination, without whom I wouldn't have had the most productive days of my life. Thank you all.

Contents

List of Figures

List of Tables

Chapter 1

Introduction

It is now well known that nearly all the galaxies in the universe contain a supermassive black hole (SMBH) at their center. The discovery of the first quasar, or active black hole, by Schmidt (1963) was the start of an increasing scientific interest in these objects. Quasars are superluminous active galactic nuclei (AGN), which are so bright that a quasar fifty light years away would be just as bright as the sun. Further study of quasars led to the theory that the light produced was the result of a hidden object about the size of the solar system but a million to a billion times the mass of the sun ($M_{\odot}$), surrounded by an accretion disk of material (Keel (1996)). The light is a result of this accretion disk, which defines it as an AGN. The existence of these quasars found in the early universe suggested that galaxies in the local universe would have remnants of these BHs in a dormant, or quiescent state. A great amount of effort was placed on finding evidence for these dormant or quiescent black holes and measuring their masses as well as evolutionary cycle (Hoyle & Fowler (1963); Salpeter (1964); Zel'dovich (1964); Lynden-Bell (1969, 1978); Lynden-Bell & Rees (1971)).

Interestingly it was not until 2019 that we were able to obtain a reconstructed image of an SMBH using the planet-sized Event Horizon Telescope (Event Horizon Telescope Collaboration et al. (2019)). However, we have been able to observe how

these SMBHs behave through the probing of their gravitational effects and the understanding of their effect on different measurable galaxy components. Studies have revealed strong correlations between the mass of the BH ($M_\bullet$) and measurable galaxy properties, such as bulge luminosity (Dressler (1989); Kormendy (1993)), bulge stellar mass (Marconi & Hunt (2003); Magorrian et al. (1998)) and bulge stellar velocity dispersion ($\sigma_\star$) (Ferrarese & Merritt (2000); Gebhardt et al. (2000)). It is, however, known that a BH does not exert a gravitational force on the whole galaxy (e.g. Valluri et al. (2004)), so these relations suggest a co-evolution of the SMBH and the host galaxy. Further investigation of these relations has found that BHs correlate differently with different components, as explained by Kormendy & Ho (2013), rather than a general correlation for all co-evolutionary components.

Evidence suggests that $M_\bullet$ relates most closely with the bulge stellar velocity dispersion ($\sigma_\star$), which is the velocity of stars relative to each other in the bulge of the galaxy (Ferrarese & Merritt (2000); Gebhardt et al. (2000). Ferrarese & Merritt (2000) and Gebhardt et al. (2000) where the first to find this relation, which was found to be so tight that all scatter could be explained through measurement error. This suggested that $\sigma_\star$ could be used as a direct measure of BH mass, a thrilling possibility as $\sigma_\star$ is much easier to measure than $M_\bullet$, especially at large distances. However, further studies (e.g. Batiste et al. (2017b); Valluri et al. (2004); Pacucci et al. (2018); Hu (2008)) revealed intrinsic scatter in the relation, giving scientists the task of finding and correcting sources of error to constrain it. Work by Onken et al. (2004) further added value to the relation, suggesting that it may hold for both quiescent and active galaxies.

Most of the error in the early stages of investigation of $M_\bullet - \sigma_\star$ was attributed to poor measurement of $M_\bullet$, which is very difficult to do. Consequently, close attention was given to refining these measurements of mass. However, even after significant improvement in $M_\bullet$ measurements, scatter in the relation remains. Evidence now

suggests $\sigma_\star$ is the dominant source of error (e.g. Batiste et al. (2017b); Bellovary et al. (2014)).

$M_\bullet$ is primarily measured using one of two methods: Reverberation Mapping (RM) or Stellar Dynamical Modeling (SDM). The most trusted method of direct detection of $M_\bullet$ is Stellar Dynamical Modeling (SDM). As explained in Batiste et al. (2017a), SDM focuses on the observation of the gravitational sphere of influence (SOI) (i.e. where the BH has a direct gravitational effect on orbiting objects) and the dynamic interaction of stars with the BH in order to extract, through the Virial Theorem, the mass $M_\bullet$. Derivations of $M_\bullet$ through this method depended on the analysis of stellar kinematics in the SOI (Dressler & Richstone (1988); Richstone et al. (1990); Valluri et al. (2004); van der Marel et al. (1998)). However, this is a significant limitation because it is necessary to be able to resolve the SOI to do SDM. The central BH only amounts to about 0.1% of the total stellar mass in its host galaxy and hence this radius of influence for a nearby galaxy corresponds to an angular size of only $0".1-1"$ (Kormendy & Ho (2013)). For AGN it becomes even more difficult to obtain SDM measurements, both because the brightness of the nucleus makes it hard to probe the stars close to the BH, and also because they are less numerous in the local universe, and hence we find a much smaller sample of AGN that are close enough to do SDM. Hence it is a method that limits the sample to nearby galaxies with an inactive, or quiescent, nucleus.

In order to measure AGN masses, the reverberation mapping (RM) Blandford & McKee (1982a) technique goes around the problem of having to observe the gravitational SOI and focuses on the luminosity variability properties of AGNs. RM exploits phenomena specific to some types of AGN, where it is possible to see spectral emission lines from gas orbiting within the BH SOI (Bahcall et al. (1972); Blandford & McKee (1982b)). $M_\bullet$ can be determined from the kinematics of this gas, via the virial theorem, but must be scaled by a multiplicative constant, f, to account for the geometry

of the gas (see discussion in Batiste et al. (2017a)). Since little is known about the distribution or morphology of this gas, f cannot be measured directly, behooving us to find a reliable method to estimate its value. Work by Onken et al. (2004) showed that f could be estimated by calibrating the $M_\bullet - \sigma_\star$ relation for AGN with that of quiescent galaxies. Therefore, a well defined $M_\bullet - \sigma_\star$ relation with a reduced error in $\sigma_\star$ is essential for accurately measuring AGN masses. This is currently the standard method for scaling RM $M_\bullet$. However, its reliability is still questioned because it is not yet clear that active and quiescent galaxies follow the same relation. In order to properly validate this method, the fit must be more tightly constrained.

Work by Batiste et al. (2017a) shows that the re-calibration of the $M_\bullet - \sigma_\star$ relation with better data for $M_\bullet$ and $\sigma_\star$ exposes an intrinsic scatter that cannot be explained by measurement error alone. We have yet to find out if there is a missing piece of fundamental understanding of this relation and whether it differs between active and quiescent galaxies and how. Some discrepancies have been found in the $M_\bullet - \sigma_\star$ relations for AGN and quiescent galaxies, as seen in Batiste et al. (2017b) and Shankar et al. (2016), but these cannot be verified, for they are statistically insignificant when accounting for sample and observational bias.

Improving our measurement of $\sigma_\star$ is the next logical step to constraining the $M_\bullet - \sigma_\star$ relation. One complication with the determination of a better $\sigma_\star$ lies in the uncertainty of its definition and lack of consistency in literature. For its determination, it is necessary to measure the galaxy's bulge effective radius, R_e, which defines the size of the bulge. $\sigma_\star$ is hence σ measured within some fraction of R_e. Definitions of the appropriate radius to use vary widely across the literature (e.g. Kormendy & Ho (2013); Batiste et al. (2017a)) with, for example, Ferrarese & Merritt (2000) using $R_e/8$ and the Nuker team (Gebhardt et al. (2000)) choosing to use R_e.

R_e is defined as the radius containing half of the galaxy's bulge luminosity, and is obtained by analyzing statistical luminosity models. Each structural component

of a galaxy emits light differently, and so it is important to take into account these structures when fitting a luminosity model. Elliptical galaxies that have minimal structure can have their luminosity fitted with a simple function, but spiral galaxies need to have their structure accounted for, or the half-light radius can be overestimated. These overestimations can be seen in large galaxy surveys such as the Atlas3D project (Cappellari et al. (2011)) which used a standard, single component, elliptical model to calculate Re for their full sample. Although generally good for elliptical galaxies, their application to spiral and even simple lenticular galaxies with more than one structural component was shown by Bentz et al. (2014) and Batiste et al. (2017b) to overestimate the true bulge R_e by at least five times (more on this in Chapter 2).

Once we have a well defined R_e, it is then necessary to measure $\sigma_\star$ within it. The kinematics of a galaxy are obtained through the use of spectroscopy, which provides information on how the galaxy, as well as the stars and gas inside it, are moving. Traditional methods of spectroscopy do not account for variations due to galaxy structure and so they add to the problem of measuring the velocity dispersion at the bulge (see Batiste et al. (2017a) for a more detailed discussion). These errors, however, can be mitigated with the use of Integral Field Spectroscopy (IFS). IFS is a spectroscopy technique that allows for the extraction of individual spectra in a subdivided field of view (FOV), which makes it possible to map the kinematics for different parts of the galaxy (see Chapter 2).

There has thus been a huge effort put into improving BH mass measurements to the point where $\sigma_\star$ is the dominant source of error. $\sigma_\star$ is measured through the bulge and we define the bulge through the effective radius. Accurate maesurement of both, the effective radius and kinematics are necessary to reduce error in $\sigma_\star$. It is thus important to see how each of these components affects our relation and our scatter in $\sigma_\star$.

This research is a continuation of the Big Reverberation-mapped AGN Velocity dispersion Examination (BRAVE) project (Batiste et al. (2017a)). The goal of this part of the project is to analyze optical IFS stellar kinematic data obtained by Cappellari et al. (2011) in their ATLAS^{3D} Project, in an effort to better constrain the $\sigma_\star$ of a sample of quiescent galaxies, with good $M_\bullet$ measurements. This would compare to the $M_\bullet - \sigma_\star$ relation published by Batiste et al. (2017a) for a sample of AGN in order to make a more consistent comparison of the statistical relation scaling of Onken et al. (2004). To do this, we perform an analysis with the help of the Galaxy IFU Spectroscopy Tool (GIST), a pipeline developed by Bittner (2021) that uses a penalized Pixel-Fitting method (pPXF; Cappellari & Emsellem (2004)) to fit the line-of-sight velocity distribution and measure the stellar kinematics. We adapt this pipeline to process data obtained with the SAURON IFU (Bacon et al. (2001)), which is the instrument used by Atlas^{3D}, as well as develop a galaxy batch processing guide, implementing it to obtain the stellar kinematics of multiple galaxies at once. A final, and most relevant objective is an analysis of the $M_\bullet - \sigma_\star$ relation for a range of effective radii at and below the proposed R_e in the Atlas^{3D} project (Cappellari et al. (2011)), in order to evaluate the effect of poor measurement of R_e in the relation.

This paper has five chapters that walk through the purpose, methods, and results of the project. Chapter two forcuses on IFS, the SAURON IFU, Voronoi Binning, pPXF, and the Atlas^{3D} project— the sample and tools that will be used to analyze the sample. Chapter three will dive into the GIST pipeline, its modifications for the use of SAURON data, and the results obtained. Chapter four is an analysis of our results, their validity, and future work.

Chapter 2

IFS, Tools, and Sample

2.1 IFU Spectroscopy

Spectroscopy is the study of light emitted and absorbed by matter. It shows the flux distribution by wavelength through the dispersion of incoming light and can tell us about the matter composition of objects by obtaining emission (peaks) and absorption (troughs) lines in the flux continuum. We may also use spectral analysis to obtain the kinematics of celestial objects through the analysis of redshift and line broadening (see section 2.2).

The traditional method of obtaining spectroscopic data is that of long slit spectroscopy (LSS). LSS obtains light from a narrow slit aperture, passing it down to a spectrograph. Light from the slit is then broken down into individual wavelength components. We can spatially resolve along the slit but not across it, meaning we are restricted by the width of the slit that light goes through. In order to extract good kinematics, it would be necessary to make multiple observations with different slit orientations and geometries as seen in Figure 2.1. This is where IFS becomes a major advantage.

(a) SDSS image without slit orientations. (b) SDSS image with the slit orientations.

Figure 2.1: Single slit orientations on the SDSS image of a target galaxy with MaNGA ID: 1-217022 as shown in Roy et al. (2021)

IFS is a spectroscopy technique that takes individual spectra at contiguous points across a field of view (FOV) of a telescope. The resulting data is in the form of a cube with (x, y, λ) as its coordinates (Figure 2.2).

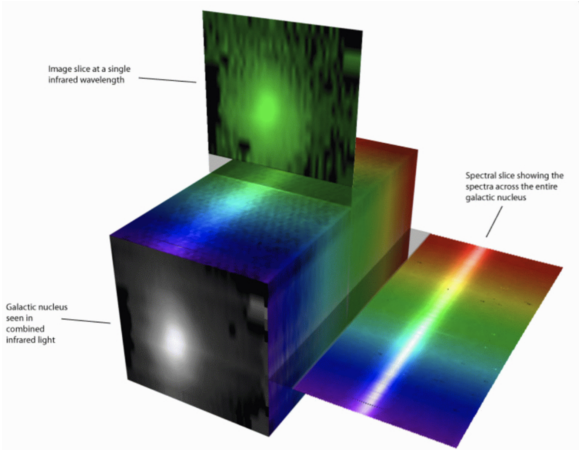

Figure 2.2: Image of an IFS datacube from the SDSS website [1]

The first attempts at the creation of an integrated field unit (IFU) were done at the ESO 3.6-m telescope by Enard et al. (1983). IFUs have since been used in a wide range of studies, such as the observation of galaxies' internal dynamics, reconstruction of gravitationally lensed galaxies, as well as the observation of star clusters and their gas density and kinematics (see Kenworthy (1998) for a more detailed review). It

[1] https://www.sdss4.org/dr16/manga/manga-tutorials/cubes-vs-rss/

has gained a lot of popularity in the past twenty years, to the point that IFUs can be found on many ground based telescopes such as the William Herschel Telescope (WHT), the Very Large Telescope (VLT), the Calar Alto Observatory (CAO) (Bacon et al. (2001); Sánchez et al. (2011); Beuzit et al. (2019); Bundy et al. (2015)), as well as the James Webb Space Telescope (JWST; Closs et al. (2008)). Some scientific highlights that relied on IFU data include the influence of dark matter in galaxies of the early universe, using the SINFONI spectrograph (Genzel et al. (2017)), or the discovery of ram pressure feeding of SMBH through the observation of jellyfish galaxies, using the MUSE IFU (Poggianti et al. (2017)).

There are different methods of constructing IFUs, but the most relevant to this research is the lenslet array technique. It makes use of a microlens array (MLA) composed of very small lenslets contiguously placed across the FOV. Each lenslet directs light into a fiber, which routes it to a spectrograph that disperses it onto a CCD (SAURON layout in Figure 2.3).

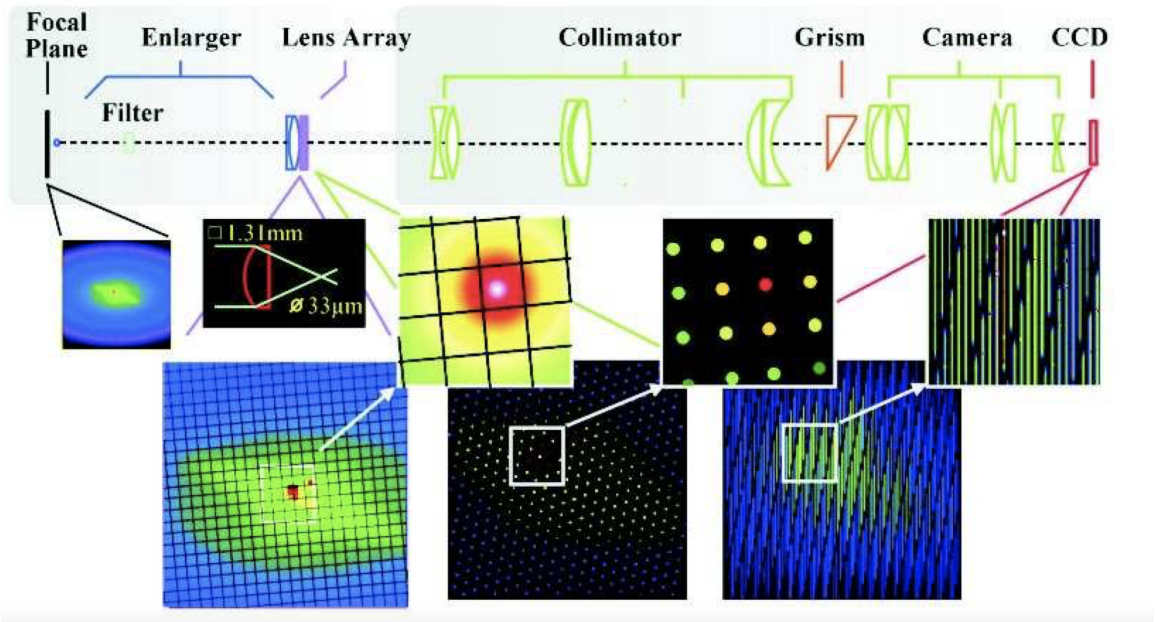

Figure 2.3: Layout of the SAURON IFU as displayed in Bacon et al. (2001)

The use of an MLA has the advantage of contiguous sampling, but this does sac-

rifice the possible wavelength viewing range. The analysis of wavelength components requires the dispersion of light on the CCD, which occupies space. The wider we want our range in wavelength to be, the more space that dispersed light will occupy. The more wavelength we want to sample from an MLA, the more space we have to sacrifice on the CCD. As mentioned in Bacon et al. (2001), the dense packing of the CCD resulted in the overlapping of the spectrum edges, as well as flux contamination. In order to be able to observe all the spectra, it is thus also necessary to sacrifice the CCD packing efficiency, since overlapping spectra cause problems when having to reduce and interpret spectral data. Therefore, this technique requires a balance between the number of spatial resolution elements and the spectral coverage.

IFS provides a spectrum for each spatial pixel, and so it is possible to map kinematics across the FOV with much better precision than is offered by the traditional long slit spectroscopy. As mentioned in Bacon et al. (2001), the traditional method of long slit spectroscopy does not provide enough spatial coverage to extract the kinematics of early-type galaxies. For a better manipulation and analysis of galaxy bulge kinematics, it is thus necessary to use IFS so as to obtain spectral data that make it possible to distinguish the kinematics in different structural components of the galaxy.

2.2 The SAURON Project

The Spectroscopic Areal Unit for Research on Optical Nebulae (SAURON) collaboration created the SAURON IFU with the purpose of studying the intrinsic shapes and kinematics, mass-to-light ratios, age and metallicity of stellar populations, as well as the frequency of kinematically decoupled cores and nuclear black holes, for a sample of nearby elliptical, lenticular, and bulges of early-type spirals (de Zeeuw et al. (2002)). It is the first robust IFS galaxy survey, producing high quality data

for galaxies within 42 Mpc in the northern hemisphere (de Zeeuw et al. (2002)).

The SAURON IFU uses a lenset array and was created based on the Time-Gated Electric field Reconstruction (TIGER) principle (Adam et al. (1989); Bacon et al. (1995); Billard et al. (2022)) to focus light through the use of a collimator, and disperse it with a grism onto a CCD. In its low resolution (LR) mode, it has a spatial sampling of 33" $\times$ 41" at 0.94" per pixel and covers the range of $4800 - 5380$ Å with the ability of simultaneous sky spectrum subtraction (Bacon et al. (2001)). It is also equipped with a high resolution (HR) mode for optimal observation nights where it can reach a sampling rate of 0.27" $\times$ 0.27" in a 9" $\times$ 11" FOV. The selected wavelength range allows for the viewing of important emission (O III, NI) and stellar absorption (Hβ, Mg b, Fe) features (Emsellem et al. (2004)) key for stellar population and kinematic analysis.

2.3 Voronoi Binning

One of the main advantages of IFS is the ability to spatially rebin data for the optimization of the signal-to-noise (S/N) ratio and the spectral resolution. It is necessary to bin the spaxels because not all the points of the galaxy are sampled at the same quality. Each spaxel will vary in its S/N, and hence some spatial elements could be useless because of a low S/N (Cappellari & Copin (2003)). Voronoi binning is an adaptive spatial binning technique that creates bins of varying size but constant S/N across the FOV. It's also equipped with the ability to maintain the natural form of the data instead of creating forced data squares, as explained by Cappellari & Copin (2003). It does so by "accreting" neighboring bins until the target S/N ratio is obtained. The importance of optimizing the S/N is that not all areas of the FOV will present the same flux. The bulge of a galaxy will be much brighter than the disk, and hence we would find a lot more noise (lower S/N) on the disk than at the

bulge. It is thus a form of reducing the bias, in the low S/N regime, that can be introduced when fitting a nonlinear physical model to the data (Cappellari & Copin (2003)). Its application is general to 2+ dimensional data and it is especially helpful for the optimization of IFS results as first seen in Verolme et al. (2003).

2.4 pPXF

Another important analysis tool that will be used to analyze the kinematics of the bins is the penalized pixel-fitting (pPXF) algorithm (Cappellari & Emsellem (2004), and improved in Cappellari (2017)). pPXF is a tool that allows for the extraction of the line-of-sight velocity distribution (LOSVD) of stars in a galaxy, where the LOSVD is expressed with a Gauss-Hermite series. It is a widely used tool, as it is effective at analyzing low S/N data, as well as data where the LOSVD is poorly sampled (more detail in Cappellari & Emsellem (2004)). The general workflow of pPXF as described in Cappellari & Emsellem (2004) begins with initial guesses of velocity (V) and velocity dispersion (σ) for the galaxy, and creates a model galaxy spectrum using a library of different stellar templates and applying a weight to each. The Gauss-Hermite best-fitting parameters are then determined through the χ^2. These polynomials adjust the width, shape, and position of the template to match the input spectrum. The information given by these parameters (h_1, h_2, h_3, h_4, ..., h_n) allows us to understand the LOSVD, where the h_1 and h_2 give V and σ, and h_3 and h_4 give statistical information on the fitting (for greater detail refer to Cappellari & Emsellem (2004)). pPXF has the advantage that it can process multiple spectra and extract the most from them, suppressing the maximum amount of noise without sacrificing quality. This makes it very advantageous for IFS data reduction and analysis (Cappellari & Emsellem (2004); Cappellari (2017)).

2.5 Atlas^{3D} and the Sample

The Atlas^{3D} project used the SAURON IFU to analyze a full sample of 276 elliptical E and lenticular S0 galaxies in the local universe. Their analysis is drawn from the observation of a complete and statistically representative parent sample of 871 nearby ($D < 42$ Mpc, $|\delta - 29°| < 35°, |b| > 15°$) galaxies, morphologically selected through visual inspection (8% E, 22% S0 and 70% S) (Atlas^{3D} I) using the Sloan Digital Sky Survey (SDSS) data release 7 (DR7). The aim of the project is to provide multicolour imaging for each galaxy, two-dimensional kinematics of the atomic (H I), molecular (CO) and ionized gas ([O III] and [N I]), together with the analysis of population and the stellar kinematics (Hβ, Fe_{5015} and Mg_b) (Cappellari et al. (2011)). The Atlas^{3D} project calculates the size of the effective radius by using photometry data from the Two Micron All Sky Survey (2MASS) and adopting an adapted Re to that provided by 2MASS. 2MASS is a sky survey dedicated primarily for the study of the large-scale structure of the Milky Way and the Local Universe (see Kleinmann (1992)). It was an infrared, ground based operation which generally will not produce high quality imaging data compared to, for example, a space telescope (e.g. Hubble Space Telescope; HST). The Atlas^{3D} project chooses to only fit a single luminosity component, disregarding any other structure. This generalization was done because the sample observed is mainly composed of elliptical galaxies, which can be well fit by a single component. It is a broad generalization that serves simplify the analysis of a large sample, but it has been shown by Batiste et al. (2017b) to overestimate the effective radii of galaxies containing structure, as many in their sample do.

In fact, even with structurally simple galaxies such as NGC 5273 (Figure 3.2g), a two component luminosity profile by Bentz et al. (2014) is necessary to properly fit the galaxy, showing that a single component gives a 5× overestimation of the effective radius (also discussed in Batiste et al. (2017b)). With more structurally complex galaxies such as NGC 3489, rigurous calculation of the effective radius by

Nowak et al. (2010) show an overestimation by Atlas^{3D} of almost 17×. Cappellari et al. (2011) thus takes a generally simple approach to calculating R_e, which sacrifices significant accuracy (more on this in chapter 4).

The subsample that will be analyzed in this project consists of lenticular (S0) and spiral (S) galaxies within the Atlas^{3D} sample, for which there is good published data of $M_\bullet$. We chose these galaxies because they contain some complex structure unlikely to be well fit by a single component luminosity function, and have been observed using the SAURON IFU, with their data publicly available. In addition to the spirals we will also be analyzing NGC 5273, an AGN studied by Batiste et al. (2017a), which will serve to compare the validity of our results. It is not analyzed by Atlas^{3D} because they did not intend to include AGN, but the data were still obtained. These galaxies and their details can be found in Table 2.1. The inital sample (see Table 2.1) is purposefully small in order to assure a working analysis that can in the future be applied to the full sample of galaxies.

ID	Classification	Central σ (km/s)	Redshift (NED)	$M_\bullet(\times 10^7 M_\odot)$	Source σ	Source $M_\bullet$
Quiescent						
NGC 2974	E4	229	0.00629	17.0 (9.55 - 20.0) +/- 0.05	de Zeeuw et al. (2002)	Compilation in Davis et al. (2017)
NGC 3489	$S0^0$(r)	138	0.00226	0.594 (0.511 - 0.678)	de Zeeuw et al. (2002)	Nowak et al. (2010)
NGC 4382	$S0^+$(s)pec	177	0.00243	1.30 (00 - 22.4)	de Zeeuw et al. (2002)	Gültekin et al. (2011)
NGC 4459	$S0^+$(r)	174	0.00398	6.96 (5.62 - 8.29)	de Zeeuw et al. (2002)	Sarzi et al. (2001)
NGC 4526	$SAB0^0$(s)	256	0.00206	47. 0 (45.6 - 48.4)	de Zeeuw et al. (2002)	Gould (2013)
NGC 4596	$SB0^+$ (r)	152	0.00631	7.67 (4.43 - 11.41)	de Zeeuw et al. (2002)	Sarzi et al. (2001)
AGN						
NGC 5276	$SA0^0$(s)	62	0.00361	$[0.5 - 2]$	Batiste et al. (2017b)	Merrell et al. (2022)

Table 2.1: Sample of galaxies selected from Atlas^{3D} with SAURON IFS data.

Chapter 3

GIST

3.1 The GIST Pipeline

The GIST pipeline (Bittner (2021)) is a convenient all-in-one IFS data analysis tool that allows for the extraction of, among other things, stellar kinematics, by exploiting the pPXF routine (Cappellari & Emsellem (2004); Cappellari (2017)). pPXF has been well used and tested in a variety of IFS projects (e.g. Cappellari (2022); Cid Fernandes (2018); Hill et al. (2022)) but does not provide an easy work-flow, especially for analyzing multiple galaxies. The integration of pPXF into this flexible and adaptable python pipeline provides the advantage of not having to, for each galaxy, separately extract a S/N ratio for each bin, voronoi rebin the spaxels, and fully adapt pPXF. This hard-coded integration of these programs provides robust simplicity in exchange for some adaptation flexibility. In addition to stellar kinematics, it can extract a variety of other useful data such as the analysis of gas kinematics and emission-line fluxes with the GandALF procedure (Sarzi et al. (2006); Falcón-Barroso et al. (2006)) and the measurement of line strength indices, as well as the corresponding stellar population properties (Kuntschner et al. (2006); Martín-Navarro et al. (2018)). All of these modules can be run independently, presenting the advantage of a compartmentalized

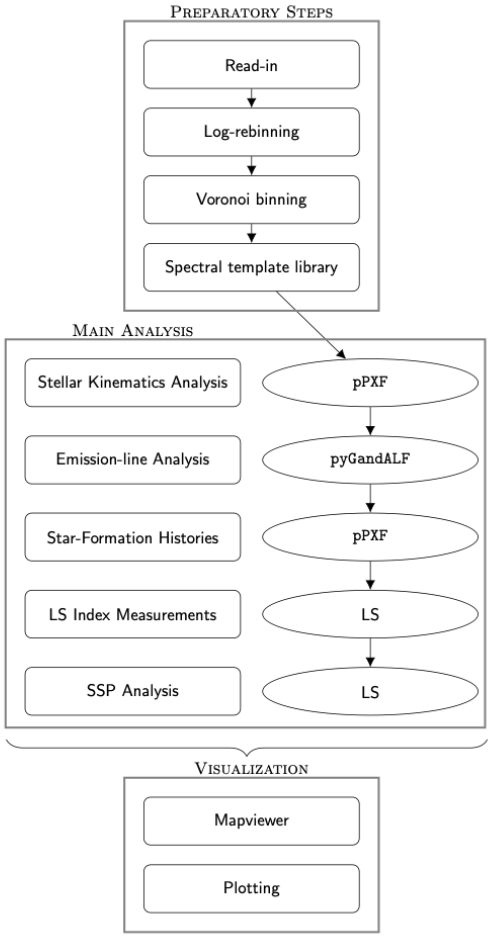

Figure 3.1: GIST Workflow as published in Bittner (2021)

work-flow and the ability to generalize for data from any IFU. This compartmentalization gives us the liberty to only make use of the stellar kinematics and plotting routine for data from the SAURON IFU (see section 3.2 for more details).

The general workflow of GIST, as seen in Fig. 3.1, begins with a master configuration file (MasterConfig), which contains the input parameters for the data that will be used, such as; the data cube used; the output data file name; the wavelength range of the instrument used; and the number of Monte-Carlo (MC) simulations that we wish to perform. These MC simulations provide a robust error estimate by simulating random noise in the data. From this MasterConfig file we also initialize the modules we're interested in. We choose only to engage the Kinematics routine for the purpose

of our project.

Once the MasterConfig file is prepared, the pipeline goes through three main stages (also seen in Fig. 3.1): Data preparation, which includes the reading of the data and creation of a GIST data cube, the log-rebinning of the wavelength, spatial rebinning to achieve the desired S/N, and the preparation of the stellar spectral templates; Main Analysis, which performs the activated routines in the MasterConfig; Visualization, which focuses on the preparation and creation of publishable plots. This publicly available code has been successfully applied to data from the MUSE, CALIFA and SINFONI IFUs as well as a variety of simulated data (Bittner (2021)), which, combined with its user friendliness, proves as a useful starting point for the analysis of SAURON IFS data.

3.2 Adaptation of GIST to SAURON

While GIST is a highly flexible pipeline designed for adaptation, there is still considerable work needed to adapt it for a completely new instrument. There were three main files that needed to be modified in order to successfully read and analyze the kinematics of the galaxies sampled by SAURON: the readData file that is part of the data preparation routine (see section 3.1), the MasterConfig, and the specMask_kin, which is the spectral mask used in the analysis of kinematics.

3.2.1 readData Routine Modifications

The specifications for a particular instrument can be done by modifying the read-in routine (readData) and the MasterConfig files. The readData module focuses on the preparation of a data cube in the form that can be used by GIST, without concern of failure due to data structure. A readData code for SAURON has not been created before, but there were templates for the MUSE IFU. The idea is to input a

data cube, extract the necessary information, and re-arrange the cube to obtain a new, standardized cube with the x, y, λ, spectra, error spectra, S/N, signal, noise, and pixel size. The main complication with adapting the MUSE readData code was that the SAURON data is flattened to two dimensions, while the MUSE data is in the form of a 3-dimensional cube. This different dimensionality turned out to be a fundamental issue, and required significant editing of several parts of the code. Some specific changes to the MUSE_WFM read-in script are the reading of this two dimensional data, the adaptation to two dimensions of the error spectra estimation, the specification of the λ, x, and y values and the transposing of the flattened data to match the necessary structure of the output cube. A copy of this code can be found in Appendix B.

3.2.2 MasterConfig Modifications

The second important set of modifications were done to the MasterConfig file. In this file we can find all the necessary specifications that allow GIST to read data and properly analyze each galaxy. This includes information proper to the SAURON instrument as well as specific to the galaxy, in addition to the file name, the MC simulation specification and the selection of the routines we wish to activate, with their own specifications. The commands that are specific to SAURON data and those specific to the galaxy analyzed are given in Table 3.1.

Specific to SAURON IFS data

Command	Value	Description
MIN_SNR	20	Spaxels below the isophote level which has this mean signal-to-noise level are masked.
TARGET_SNR	60	Target signal-to-noise ratio for the Voronoi binning.
METHOD	SAURON_LR	Name of the routine in spatialMasking/ (without .py) to perform the tasks. Set 'False' to turn off module.
ORIGIN	0, 0	Origin of the coordinate system in pixel coordinates: x,y (Indexing starts at 0).
LMIN_TOT	4800	Spectra are shortened to the rest-frame wavelength range defined by LMIN_TOT and LMAX_TOT.
LMAX_TOT	5300	Note that this wavelength range should be longer than all other wavelength ranges.
LMIN_SNR	5071.5	Rest-frame wavelength range used for the signal-to-noise calculation [in Angst.]
LMAX_SNR	5075.5	
VELSCALE	105	Spectral sampling of the logarithmically rebinned spectra [in km/s]; e.g. velscale = dLambda*C / mean(wave), with the spectral sampling of the linearly binned spectra dLambda, the speed of light C, and the mean wavelength of the spectrum mean(wave).

Specific to the Galaxy Analyzed

Command	Description
RUN_ID	Name of the analysis run. A subdirectory of this name within the output directory will be created.
INPUT	Input file for this analysis run. The specified path is relative to the input path given in defaultDir.
REDSHIFT	Initial guess on the redshift of the system [in z]. Spectra are shifted to rest-frame, according to this redshift.
SIGMA	Initial guess of the velocity dispersion of the system [in km/s].
MC_PPXF	Number of Monte-Carlo simulations to extract errors on the stellar kinematics. Formal errors are saved in any case.

Table 3.1: Table with commands specific to SAURON IFS data with their corresponding values and commands specific to the galaxy analyzed. The latter values for each galaxy can be found in Table 2.1. The description is taken as-is from the GIST MasterConfig file (Bittner (2021))

Overall, the modifications of these commands can have a large impact on the results. It is necessary to give pPXF an initial guess of σ (as explained in section 2.2) as well as give a target S/N to which all bins will be normalized. These two values are important for the results and can cause significant bias if not determined correctly. As an example, when analyzing NGC 3489 a slight, but significant, difference in results was found for an overestimation of σ of 30 ($km \cdot s^{-1}$) compared with the published Atlas^{3D} value. The target S/N ratio can be measured by finding a relatively flat piece of the galaxy's spectrum, which must also be inputted in the LMIN_SNR/LMAX_SNR. For SAURON, the optimal TARGET_SNR we found was 60. A lower TARGET_SNR will not bin the spaxels correctly (a target of 40 for NGC 4382 was not enough to produce physical results) and a higher target will simply reduce the resolution of the data and the number of spaxels, without adding quality to the results (the bins for a target over 60 were too sparse). A sample MasterConfig file for a SAURON-observed galaxy can be found in Appendix C. This can also be used as a template, where the necessary adaptations specific to the galaxy can be

found in Table 3.1.

3.2.3 Spectral Masking

In addition to the reading and configuration files that need to be modified, it is sometimes helpful with pPXF to use a spectral mask. The spectral mask is used to block certain specified regions of the spectrum and disregard the analysis for such. Since we want to focus only on the bulge stellar kinematics, we want to analyze the region of the spectrum that contains mostly stellar features. There are two ways this can be done: masking out gas emission lines, or only using the areas of strong stellar absorption features and masking out the rest of the spectrum. We can specify in the specMask_kin file what we want to mask from the spectrum (i.e. the wavelength and width of the spectral mask). Multiple ranges can be applied. We tested both and found that choosing only the strong stellar absorption features (Hb, Mg b, Fe) resulted in a worse fit than running pPXF with only the emission lines masked, so we chose to only mask the [O III] emission lines (a bestfit overlay for our results can be found in Appendix A).

Our data analysis was done using the sample MasterConfig in Appendix C where the only changes were those specific to the galaxy (i.e. Table 3.1, using values from Table 2.1) as well as the MILES library (Vazdekis et al. (2010)) for the stellar templates. We also used the adapted readData routine, SAURON_LR (see Appendix B), for the creation of the data cube used in the stellar kinematics module of GIST.

3.3 Batch Processing

A significant objective of the project was to be able to batch process a subset of galaxies in an automated way. This was made easier by the fact that galaxies in the sample all shared a similar region of continuity in the flux at the de-redshifted

wavelength range of 5071.5 - 5075.5 Å. The approach taken required a .csv file containing the information to be edited for each galaxy: the RUN_ID, the INPUT file, the REDSHIFT, SIGMA, and the desired number of MC simulations. I then wrote code to replace these values for each galaxy within a template MasterConfig file (see Appendix C). The REDSHIFT for each galaxy was obtained from NASA/IPAC Extragalactic Database (NED [1]) and an initial estimate of σ taken from the SAURON PII (de Zeeuw et al. (2002)) early results.

Since results are sensitive to the initial guess of σ, we found that an iterative extraction of σ might be a good way to obtain better results. The simple batch processing (Appendix B) was hence also transformed into a more developed version that does multiple runs of pPXF at 0 MC simulations to extract and replace the median value of σ, followed by one final run at 100 MC simulations. The infrastructure of this code is the same as its simplified version, offering a way to easily constrain the initial guess of σ. It must be noted that, although functional, the analysis of our reduced sample was not done using this iterative code due to the objective of the project focusing on the effects of effective radii on $\sigma_\star$. As will be covered in Chapter 4, we find a systematically higher central σ as well as $\sigma_\star$ but this did not intervene with our ultimate objective (see Table 4.1 for numerical results).

3.4 Results

We ran the SAURON adaptation of GIST for our subset of galaxies to extract the first four Gauss-Hermite moments (h_1:V, h_2:σ, h_3, h_4) and exploited the interactive mapping routine to obtain the kinematic maps of each galaxy in our sample. After finding no significant difference in the error estimate for 10 and 100 MC simulations, we chose to not go higher than 100. The sample of quiescent galaxies can be seen in Figures 3.2a - 3.2f and the AGN NGC 5273 in Fig 3.2g. An example spectrum for

[1] https://ned.ipac.caltech.edu

each galaxy with the pPXF best fit overlayed is given in Appendix A.

Figure 3.2: Kinematics for every galaxy in the sample. We extracted the first four Hermit coefficients: Velocity (V, top left), velocity dispersion (σ, top right), h_3 and h_4. Max and min values are shown for each map.

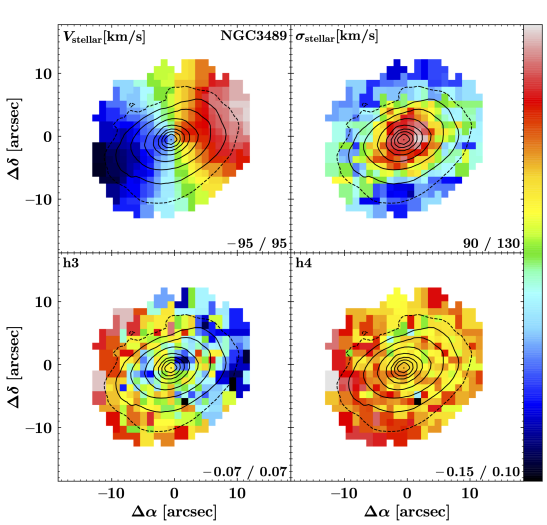

(a) NGC 3489

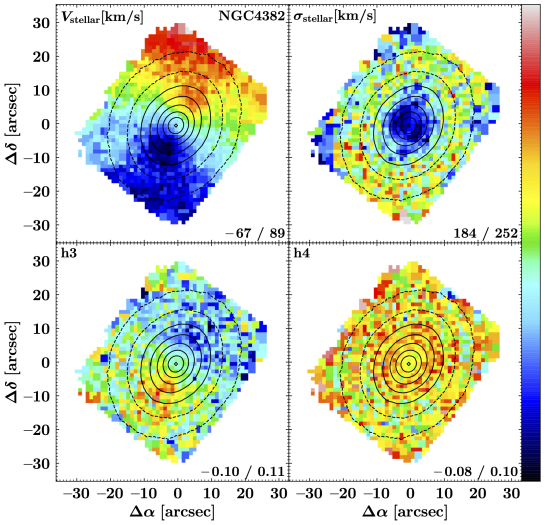

(b) NGC 4382

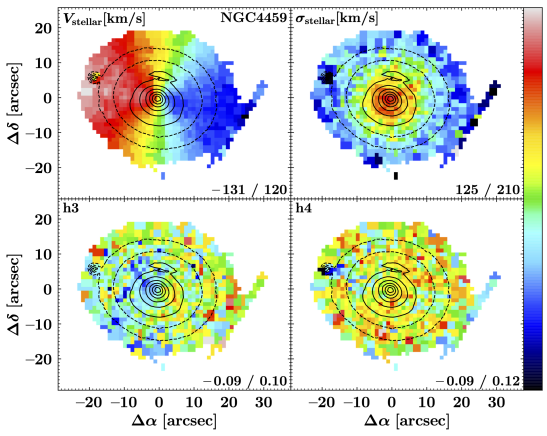

(c) NGC 4459

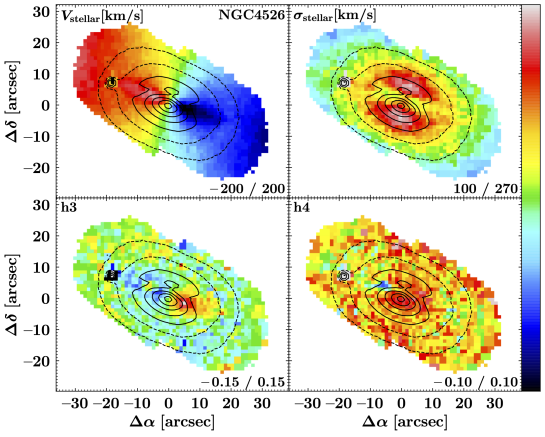

(d) NGC 4526

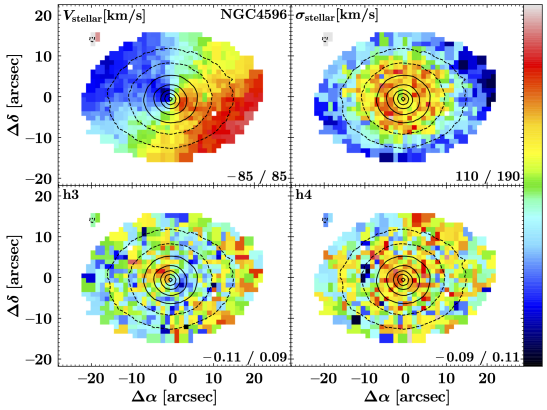

(e) NGC 4596

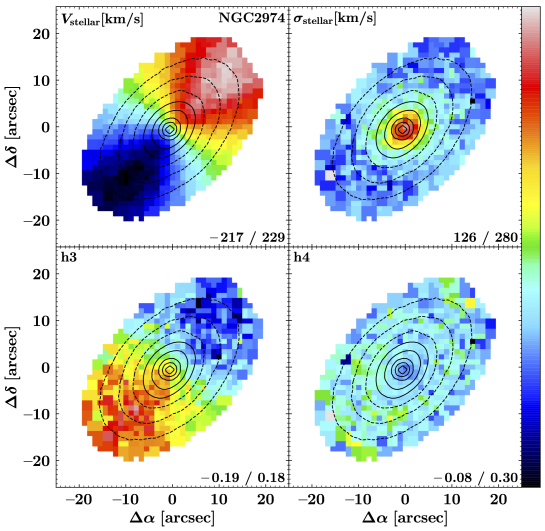

(f) NGC 2974

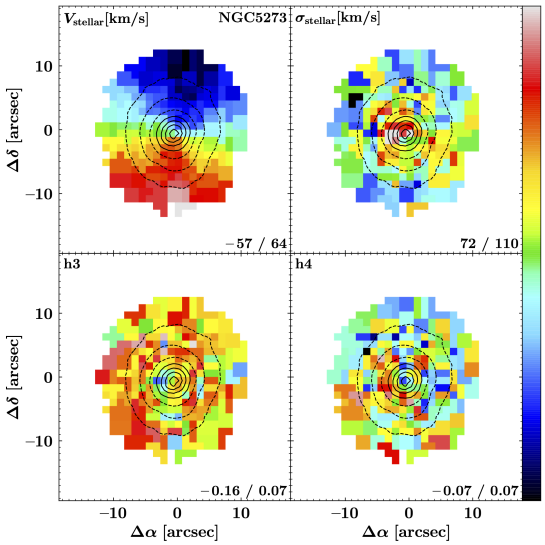

(g) NGC 5273

The AGN galaxy NGC 5273 was accidentally observed by the SAURON team in their analysis of early-type, inactive galaxies. However, it proved to be a very useful source of comparison between the Atlas^{3D} effective radius and $\sigma_\star$ to point out its overestimation. It is also a useful test to check our results in comparison to the pPXF analysis by Batiste et al. (2017b), and have another point of comparison for the validity of GIST. NGC 5273 is a lenticular AGN galaxy with minimal structure (see

Figure 3.3a). Our results for this galaxy showed a small number of high σ components in the central region of the galaxy that do not show up in the velocity maps of Batiste et al. (2017b). Our stellar velocity dispersion is slightly higher than the results by Batiste et al. (2017b) which may be due to some differences in our analysis method (see Chapter 4 for more discussion and Figure 3.3b for Batiste et al. (2017b) results).

Figure 3.3: NGC 5273: HST image and result comparison for σ

(a) HST image.

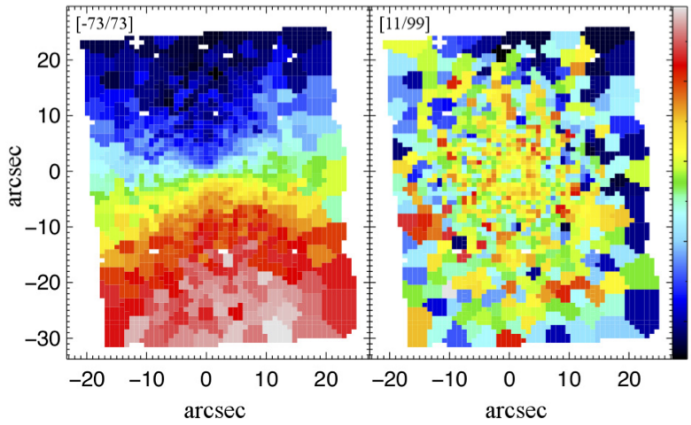

(b) V (left) and σ (right) results from Batiste et al. (2017b)

The results for NGC 3489, NGC 4459, NGC 4526, NGC 4596 align with those obtained by Emsellem et al. (2004) in their kinematic analysis. Some outstanding morphological and kinematic features that appear and were mentioned are the "kinematically decoupled components (KDCs), showing either a twist in the nuclear kinematic axis or a central velocity field" (Emsellem et al. (2004)) as we can see in NGC 4382, and the dumbbell shaped σ field in NGC 4526 due to a fast rotating stellar component (Emsellem et al. (2004)) that is visible in the velocity map between $\Delta\alpha = -20" - -10"$ (shown in Pellegrini, Held and Ciotti (1997)). We see a similar depression in the velocity field of NGC 4459 as well as a branch of unusually low velocity dispersion between $\Delta\alpha = 20" - 30"$. This depression in the velocity field was not mentioned in the results by Emsellem et al. (2004) but it does appear in their kinematic maps. The branch does not appear in their results, because the FOV is

cut off to exclude that region.

While there are some variations, our results are consistent with those of Emsellem et al. (2004), and therefore validate GIST and its use with SAURON data. We can use these results now to analyze the kinematics at a variety of effective radii and see how the effective radius affects the $M_\bullet - \sigma_\star$ relation.

Chapter 4

Analysis

The sample we chose to analyze is composed of galaxies that show some sort of structure that is unlikely to be well fit by a single componenet luminosity function. Images of these galaxies can be found in Figure 4.1 as well as an overlay of the different effective radii that will be analyzed (discussed in 4.1).

Figure 4.1: HST images of our quiescent sample with different effective radius estimations as seen on the scaling bar: the Atlas^{3D} radius Re_A (blue), as well as $Re_A/5$ (red) and $Re_A/17$ (green).

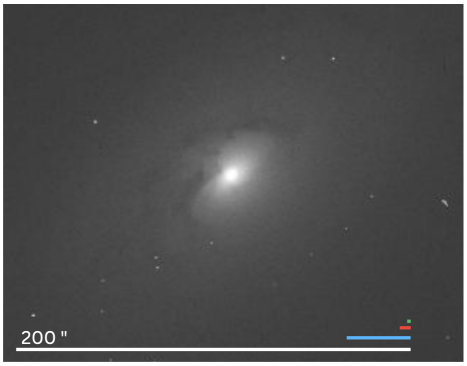

(a) NGC 2974

(b) NGC 3489

(c) NGC 4382

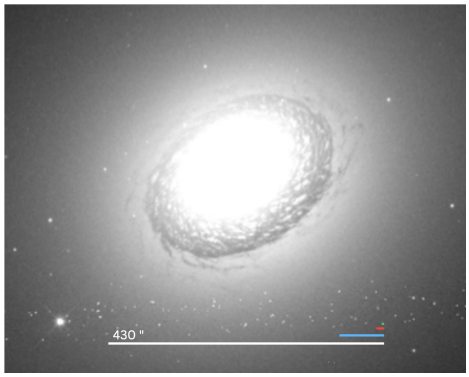

(d) NGC 4459

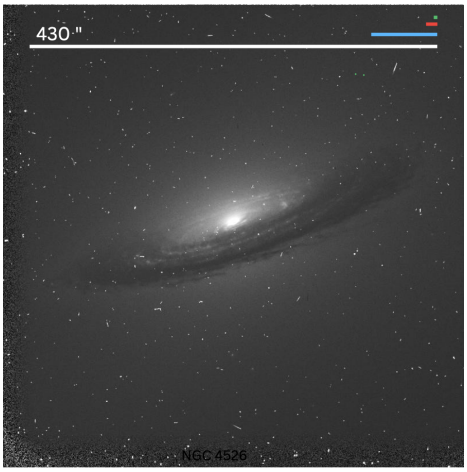

(e) NGC 4526

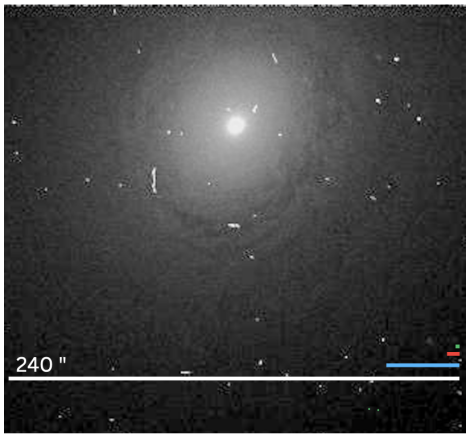

(f) NGC 4596

4.1 Effective Radii Analysis

Research focusing on galaxy luminosity profiles has directly and indirectly shed light on the overestimation of the effective radii by the Atlas^{3D} project. Work by Bentz et al. (2014) and Batiste et al. (2017b) has shown that for NGC 5273, a lenticular AGN with minimal structure, the effective radius was overestimated by about 5×. For galaxies with more complex structure this issue is even more pronounced. Nowak et al. (2010) show in their work that in the case of the lenticular galaxy NGC 3489, the

photometric bulge could be decomposed further. The photometric bulge was found to be a predominantly "disk-like" bulge known as a pseudo-bulge, accompanied by a much smaller central light excess which they determine to be a "classical bulge". The isophote analysis of NGC 3485 showed, for the photometric bulge, a radius 5× smaller than the Atlas^{3D} results, and a classical bulge 17× smaller. Even with simple elliptical galaxies, as is the case for NGC 2974, an independent decomposition of the brightness profile done by Davis et al. (2019) further adds to the evidence, finding a half-light radius almost 6× smaller than the Atlas^{3D} published value. This is evidence enough to believe that the $\sigma_\star$ calculated by Atlas^{3D} takes into account a bulge that is at least 5× larger, and could be up to 17× overestimated in the case of galaxies with pseudo-bulges. It was possible to adapt the mapping routine present in GIST to match bins to their corresponding kinematics and extract the kinematics of the galaxy at different radii of choice (see Appendix B) to investigate the effects on $\sigma_\star$. Here (Figure 4.2) we find the $M_\bullet - \sigma_\star$ relation for our sample of quiescent galaxies using a range of different R_e to investigate the effects of the systematic overestimation on the measured $\sigma_\star$ and the resulting fit to the $M_\bullet - \sigma_\star$ relation. The numerical values for the different $\sigma_\star$ calculated along with the Atlas^{3D} published values can be seen in Table 4.1.

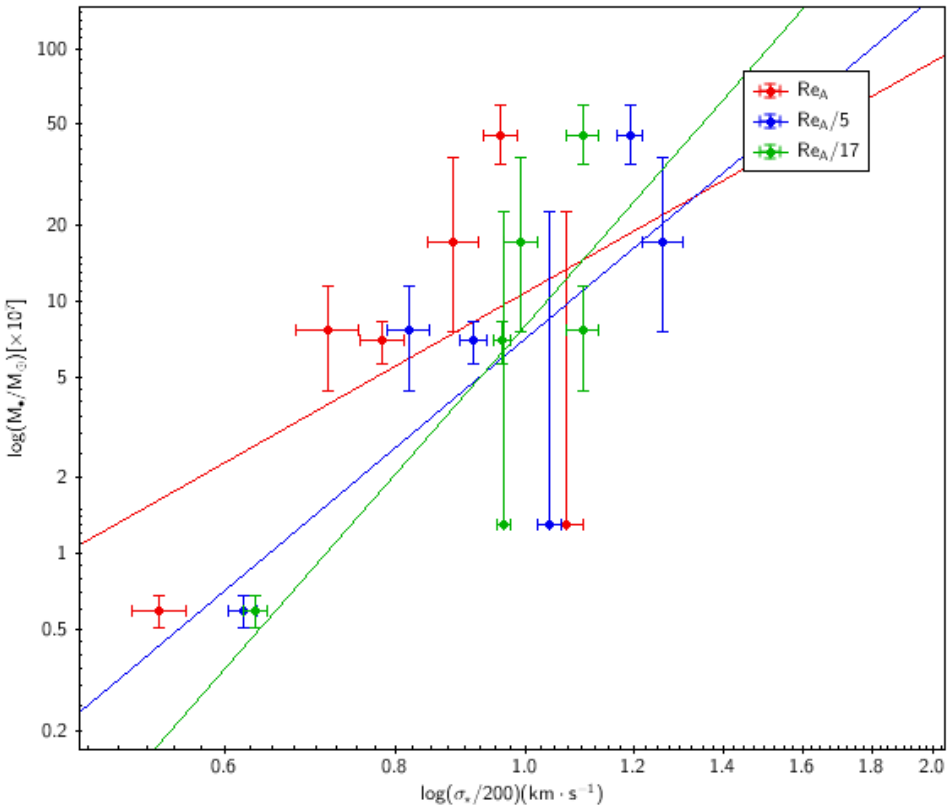

Figure 4.2: The $M_\bullet - \sigma_\star$ relation for our sample of quiescent galaxies on a logarithmic scale. Re_A refers to the estimation of effective radii done by Cappellari et al. (2011).

ID	Published $\sigma_\star$ (km/s)	GIST $\sigma_\star$ (km/s) at Re_A	GIST $\sigma_\star$ (km/s) at $Re_A/5$	GIST $\sigma_\star$ (km/s) at $Re_A/17$	Source Published $\sigma_\star$
Quiescent					
NGC 2974	226.46	176.53	252.54	198.33	Cappellari et al. (2013a)
NGC 3489	101.16	107.15	123.80	126.21	Cappellari et al. (2013a)
NGC 4382	179.06	214.45	207.95	192.51	Cappellari et al. (2013a)
NGC 4459	158.12	156.59	182.72	192.05	Cappellari et al. (2013a)
NGC 4526	208.93	191.25	239.21	220.39	Cappellari et al. (2013a)
NGC 4596	125.60	142.87	163.82	220.39	Cappellari et al. (2013a)
AGN					
NGC 5276	66.68, 62	89.86	93.08	100.30	Cappellari et al. (2013a), Batiste et al. (2017b)

Table 4.1: GIST results at different scales of the Atlas^{3D} published effective radii as well as the published values for $\sigma_\star$ in Atlas^{3D}. The second value of $\sigma_\star$ for NGC 5273 is found in Batiste et al. (2017b) using a different effective radius than for the Atlas^{3D} publications.

Figure 4.2 presents a fitting of the $M_\bullet - \sigma_\star$ relation for different scales of the published radii by Atlas^{3D} (Re_A). We see a progressive tightening of the trend as we reduce the radius to the photometric ($Re_A/5$) and classical ($Re_A/17$) bulge size

estimations. We can see that, even though the trend tightens, the change in $\sigma_\star$ is not systematic as we reduce our radius (as seen for NGC 4526 or NGC 4382). This indicates that the choice of effective radius is contributing to the scatter in $M_\bullet - \sigma_\star$ and improved measurements of R_e are key to reduce such scatter. A careless selection of effective radius would be contributing to the scatter of the relation, hiding the true fit.

One of the effects that can cause these changes in $\sigma_\star$ is the viewing angle of the galaxy. As seen in Figure 4.1, some galaxies are face-on (e.g. NGC 4459) and some are more edge-on (e.g. NGC 4526). Simulations have shown that the observed kinematics of these galaxies are biased to the line of sight (e.g. Bellovary et al. (2014)). For more edge-on galaxies, the disk of the galaxy can obscure bulge kinematics and prevent us from truly measuring σ in the bulge. Bellovary et al. (2014) shows that the distribution of the velocity dispersion along the line of sight (LOS) skews higher at more inclined orientations. They also find that the added scatter due to highly inclined galaxies could explain almost all of the scatter at the low-mass end of the $M_\bullet - \sigma_\star$ relation.

A different relation has also been hypothesized for galaxies with and without pseudo-bulges where Hu (2008) shows contrasting relations, indicating that the formation and growth histories of the SMBH depends on whether or not a pseudo-bulge is present. This is one of the elements that adds confusion in the definition of $\sigma_\star$. Would we need to define $\sigma_\star$ as the photometric/pseudo-bulge, or the "classical", smaller bulge? This very small sample suggests that the use of a classical bulge correlates better, but it would be necessary to analyze a larger sample to obtain statistically significant results. Further studies have also seen discrepancies between the low-mass end and high-mass end of the relation (see Pacucci et al. (2018); Hu (2008); Bellovary et al. (2014) for a more detailed explanation), but this sample is insufficient to probe that possibility.

To further understand the trend, we fit the $M_\bullet - \sigma_\star$ relation with the published effective radii for NGC 3489, NGC 2974, and NGC 5273 and choose to scale the rest of the sample down by 5 based on the work of Batiste et al. (2017b) (see Figure 4.3a).

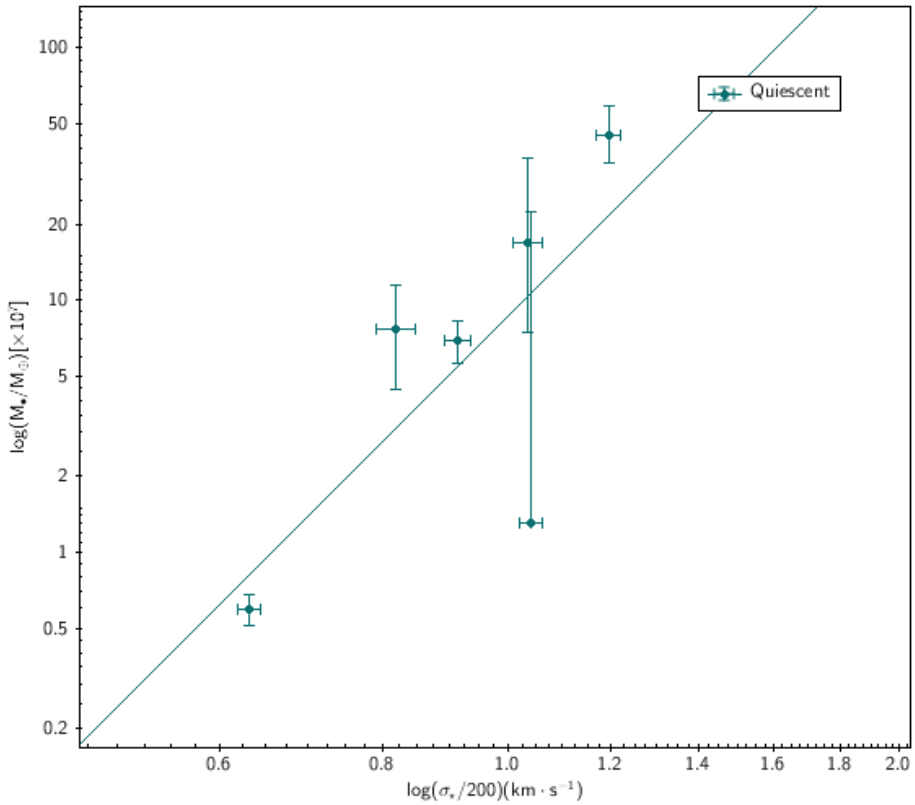

(a) Adapted $M_\bullet - \sigma_\star$ relation using the published effective radii for NGC 3489 and NGC 2974.

The adaptation of effective radius done in Figure 4.3a results in a tighter fit than when using the Atlas^{3D} effective radii. There is also a noticeably skewed galaxy for which the mass is only a lower limit (NGC 4382), which could further contribute to the scatter in our plots. We can see just how much this galaxy skews our results when plotting the relation without it (see Figure 4.3b). Even though our quiescent sample is too small to obtain significant results, we still find coefficients in Figure 4.3a that almost perfectly match those published by Batiste et al. (2017b) for their sample of quiescent galaxies while largely reducing the scatter. For a fit in the form of $\log(M_\bullet/M_\odot) = m\log(\sigma_\star/200) + c$, our m and c coefficients are 5.15 and 8.61 and

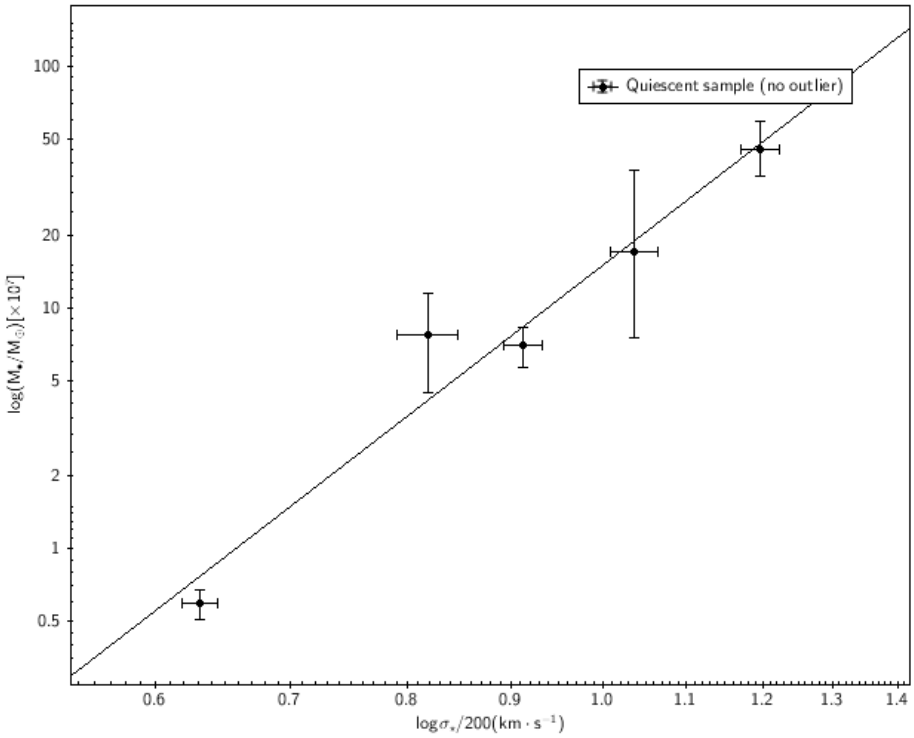

(b) $M_\bullet - \sigma_\star$ relation removing the outlier in our sample NGC 4382 using the same effective radii as Figure 4.3a

those by Batiste et al. (2017b) 5.32 ± 0.63 and 8.55 ± 0.09. However, with Figure 4.3b, we find very different coefficients from the published values but a much tighter (almost perfect) fit with a deviation from the trend of 0.14 compared to the earlier at 0.44. In this case, the coefficients are 6.46 and 15.1 for m and c respectively. For both cases we did not have a sample significant enough to include a representative error calculation for the coefficients. Still, the slope and offset for Figure 4.3b is out of the error bounds published by Batiste et al. (2017b). Regardless of these differences, the results show that the choice of effective radius could indeed be the currently dominating source of scatter in the relation and should be better understood if we want to obtain physically meaningful results.

Our estimations of $\sigma_\star$ were done by taking a median value of our velocity dispersion at a certain effective radius. We do find our values of $\sigma_\star$ to be systematically higher when compared to the published values by Batiste et al. (2017b) and in the Atlas^{3D}

paper 15 and 20 (AP15, AP20; Cappellari et al. (2013b)). AP15 finds effective velocity dispersions at their published $R_e/8$ by co-adding the spectra contained within their estimation of effective radius. They then re-fit these spectra with pPXF. This is a much more robust method of calculating $\sigma_\star$ as it limits pPXF to only analyzing the areas of interest without considering in its calculations other affecting morphological factors (further explained in section 4.2). Work by Batiste et al. (2017b) on NGC 5273 using a similar method, also finds agreeing $\sigma_\star$ values with those published in Atlas^{3D} P15.

4.2 Future Work

In this project we settle a foundation for the further study of galaxies observed with the SAURON IFU, with the use of GIST. However, there are some limitations to GIST and our method of analysis that we recommend be fixed or investigated for the future.

A limitation of GIST is its adaptation of pPXF which leaves out some of its versatility in exchange for user interface simplification. Two main features that stand out that would be useful to obtain better calculations of $\sigma_\star$ are the possibility of choosing only a subset of the star templates for the best fit, and the ability to reject possible outliers from the spectra (discussed in AP15 and in a private conversation with Dr. Batiste).

If not determined otherwise by the user, pPXF executes a best fit using all the templates in the stellar template library defined. A conversation with Dr. Batiste revealed that the best fits do not result from the use of every template but rather the few most heavily weighted ones. This is something that can be changed when executing pPXF independently, but that was not integrated into GIST. The possibility of adding to GIST the flexibility to choose the best templates and re-run an itera-

tive process could be a significant contribution that would allow for more physically meaningful results.

As mentioned in our analysis, our central σ results are systematically higher than those published by Batiste et al. (2017b) and Cappellari et al. (2013b) but they are still valid and show the promising idea that the effective radius measurements do contribute to the scatter in the relation. One way to better obtain $\sigma_\star$ would be by taking a luminosity weighted average instead of the median value of the bins. By doing this we would give more value to those bins that have a higher S/N. Another method would be integrating the spectra within the effective radius, combined with an iterative σ extraction routine. For the latter, we present an iterative code that extracts and replaces estimated median σ values to input into pPXF as a first guess. This routine, however cannot deal with outliers in the data cube (as seen in the kinematics of NGC 4459 and NGC 4596). Anywhere in our data cube where data is bad can change the template selection by pPXF. As mentioned in AP15, pPXF has a keyword (CLEAN) that allows the user to reject possible outliers. One way to work around outliers would be by manually finding and removing the bins that are unwanted and re-fitting the spectrum with pPXF, as was done in the calculation of the effective velocity dispersion by Batiste et al. (2017b) and Cappellari et al. (2013b).

Interesting future work would involve the batch processing of a larger sample of galaxies to find a statistically significant value for the $M_\bullet - \sigma_\star$ relation coefficients as well as the development of code that automates the calculation of $\sigma_\star$ within various effective radii for an arbitrary number of galaxies. The code provided (see Appendix B) requires a manual extraction of these values, which can become tedious for larger samples.

In this project we lay the foundation and provide the necessary elements for the future analysis of SAURON IFS data with GIST. We present the limitations of GIST as well as a variety of codes useful for the analysis of $\sigma_\star$ that can be scaled for larger

sample analysis. We find that the choice of effective radius has a considerable effect in the scatter of $\sigma_\star$ and should be a point of scientific focus if we wish to constrain the $M_\bullet - \sigma_\star$ relation.

Appendix A

pPXF Best Fit Results

Figure A.1: pPXF best fit overlayed with a sample observed spectrum, choosing BIN 0, or the central position of every galaxy. It was extracted using the GIST Mapviewer routine. The black line represents the observed spectrum, in red the pPXF fitted spectrum and in green the residuals. The light gray boxes are the spectral masks for the [O III] lines.

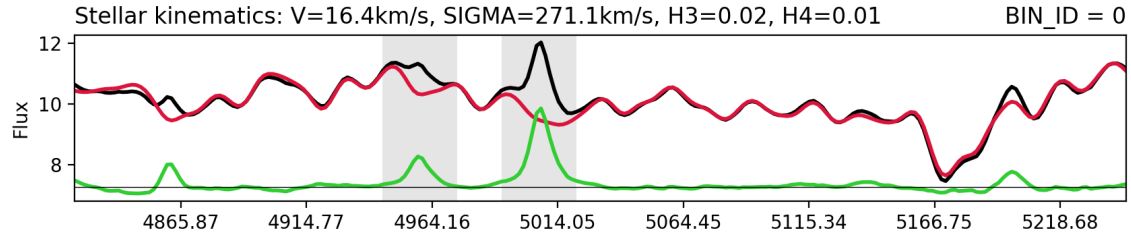

(a) NGC 2974

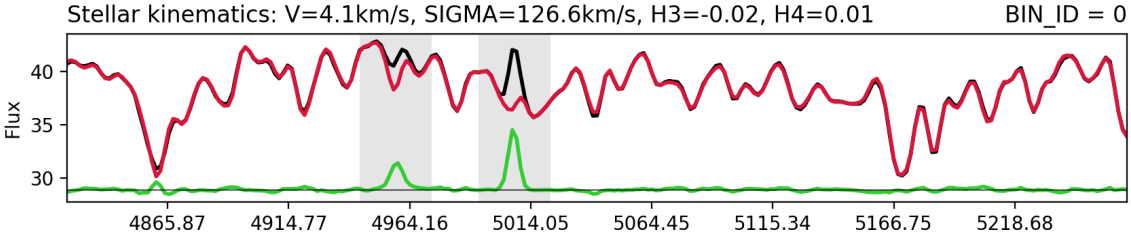

(b) NGC 3489

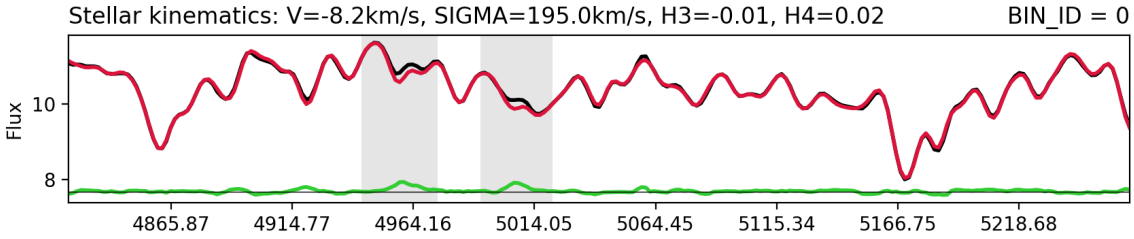

(c) NGC 4382

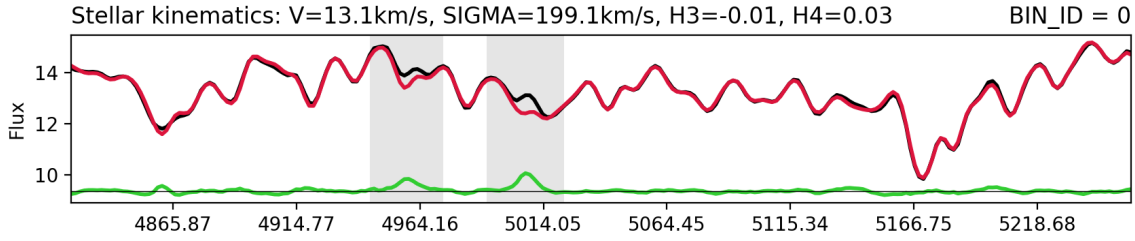

(d) NGC 4459

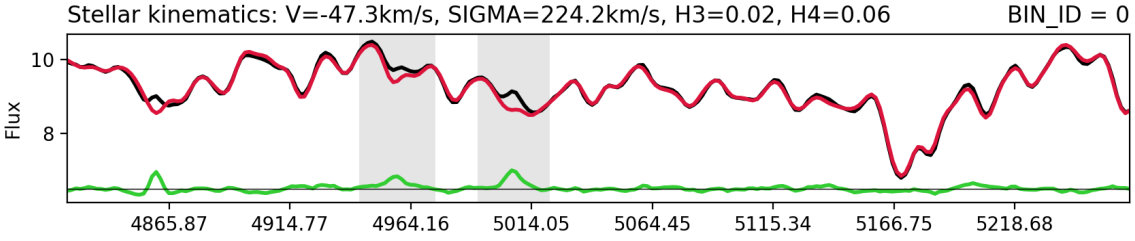

(e) NGC 4526

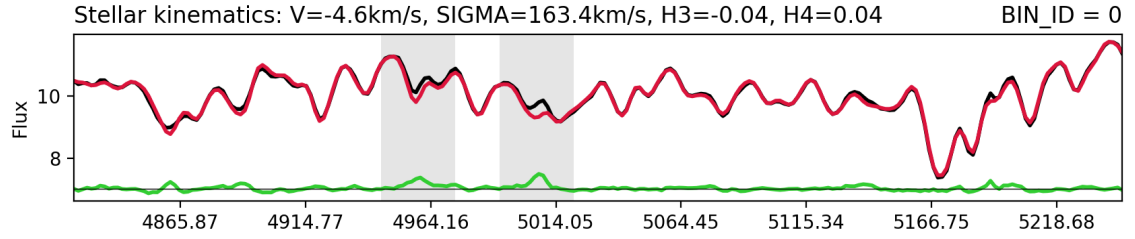

(f) NGC 4596

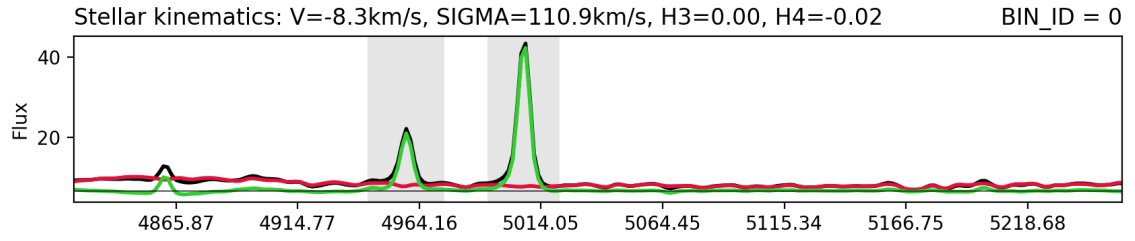

(g) NGC 5273

Appendix B

Analysis Codes

Code Listing B.1: SAURON_LR read-in routine inspired on the MUSE_WFM routine in GIST. This code must be placed in the readData directory of GIST. It is compatible with the recommended python version of GIST (Python 3.6)

```
from astropy.io  import fits
import numpy  as np
import os
import logging

from printStatus import printStatus

from gistPipeline.readData    import der_snr as der_snr




# ======================================
# Routine to set DEBUG mode
# ======================================
def set_debug(cube, xext, yext):
```

```
    logging.info("DEBUG mode is activated. Instead of the entire
                                        cube, only one line of spaxels
                                         is used.")
    cube['x']      = cube['x']     ][  int(yext/2)*xext:(int(yext/2)+
                                        1)*xext]
    cube['y']      = cube['y']     ][  int(yext/2)*xext:(int(yext/2)+
                                        1)*xext]
    cube['snr']    = cube['snr']   ][  int(yext/2)*xext:(int(yext/2)+
                                        1)*xext]
    cube['signal'] = cube['signal'][  int(yext/2)*xext:(int(yext/2)+
                                        1)*xext]
    cube['noise']  = cube['noise' ][  int(yext/2)*xext:(int(yext/2)+
                                        1)*xext]

    cube['spec']   = cube['spec'  ][:,int(yext/2)*xext:(int(yext/2)+
                                        1)*xext]
    cube['error']  = cube['error' ][:,int(yext/2)*xext:(int(yext/2)+
                                        1)*xext]

    return(cube)

# ======================================
# Routine to load SAURON-cubes
# ======================================
def readCube(config):

    loggingBlanks = (len( os.path.splitext(os.path.basename(__file__
                                        ))[0] ) + 33) * " "

    # Read SAURON-cube
    printStatus.running("Reading the SAURON cube")
    logging.info("Reading the SAURON cube: "+config['GENERAL']['
                                        INPUT'])
```

```
# Reading the cube
hdu    = fits.open(config['GENERAL']['INPUT'])
hdr    = hdu[1].header
data = hdu[1].data
coord   = hdu[2].data
s      = np.shape(data)
spec   = hdu[0].data

# Read the error spectra if available. Otherwise estimate the
                                    errors with the der_snr
                                    algorithm
if len(hdu) == 4:
    logging.info("Reading the error spectra from the cube")
    stat   = hdu[2].data
    espec = np.reshape(stat,[s[0],s[1]*s[2]])
elif len(hdu) == 3:
    logging.info("No error extension found. Estimating the error
                                        spectra with the der_snr
                                       algorithm")
    espec = np.zeros( [spec.shape[0],spec.shape[1]] )
    for i in range( 0, spec.shape[1] ):
        espec[:,i] = der_snr.der_snr( spec[:,i] )

# Getting the wavelength info
wave = hdr['CRVAL1']+(np.arange(s[1]))*hdr['CDELT1']

# Getting the spatial coordinates -- For origin CHECK MASTER
                                    CONFIG
origin = [ float(config['READ_DATA']['ORIGIN'].split(',')[0].
                                    strip()), float(config['
                                    READ_DATA']['ORIGIN'].split(',
                                    ')[1].strip()) ]
```

```
x = coord["A"]
y = coord["D"]
pixelsize = hdr['CDELT1']

logging.info("Extracting spatial information:\n"\
        +loggingBlanks+"* Spatial coordinates are centred to "+
                                            str(origin)+"\n"\
        +loggingBlanks+"* Spatial pixelsize is "+str(pixelsize))

# De-redshift spectra
wave = wave / (1+config['GENERAL']['REDSHIFT'])
logging.info("Shifting spectra to rest-frame, assuming a
                                    redshift of "+str(config['
                                    GENERAL']['REDSHIFT']))

# Shorten spectra to required wavelength range
lmin  = config['READ_DATA']['LMIN_TOT']
lmax  = config['READ_DATA']['LMAX_TOT']
idx   = np.where( np.logical_and( wave >= lmin, wave <= lmax ) )
                                     [0]
# Transpose the data axes
spec  = spec.T
espec = espec.T

spec  = spec[idx,:]
espec = espec[idx,:]
wave  = wave[idx]
logging.info("Shortening spectra to the wavelength range from "+
                                    str(config['READ_DATA']['
                                    LMIN_TOT'])+"A to "+str(config
                                    ['READ_DATA']['LMAX_TOT'])+"A.
                                    ")
```

```
# Computing the SNR per spaxel
idx_snr = np.where( np.logical_and( wave >= config['READ_DATA'][
                                    'LMIN_SNR'], wave <= config['
                                    READ_DATA']['LMAX_SNR'] ) ) [0
                                    ]
signal  = np.nanmedian(spec[idx_snr,:],axis=0)
if len(hdu) == 4:
   noise  = np.abs(np.nanmedian(np.sqrt(espec[idx_snr,:]),axis=0
                                       ))
elif len(hdu) == 3:
    noise = espec[0,:]
snr    = signal / noise
logging.info("Computing the signal-to-noise ratio in the
                                    wavelength range from "+str(
                                    config['READ_DATA']['LMIN_SNR'
                                    ])+"A to "+str(config['
                                    READ_DATA']['LMAX_SNR'])+"A.")

# Storing everything into a structure
cube = {'x':x, 'y':y, 'wave':wave, 'spec':spec, 'error':espec, '
                                    snr':snr, 'signal':signal, '
                                    noise':noise, 'pixelsize':
                                    pixelsize}

# Constrain cube to one central row if switch DEBUG is set
if config['READ_DATA']['DEBUG'] == True: cube = set_debug(cube,
                                    s[2], s[1])

printStatus.updateDone("Reading the SAURON cube")
print("              Read "+str(len(cube['x']))+" spectra!")
logging.info("Finished reading the SAURON cube! Read a total of
                                    "+str(len(cube['x']))+"
                                    spectra!")
```

```
    return(cube)
```

Code Listing B.2: This is a simple code to batch process a set of SAURON-observed galaxies. It is necessary to run this code from your python environment that contains GIST.

```
import numpy as np
import pandas as pd
import os

# shell comands

cd = 'cd INSERT DIR HERE' #choose directory where csv table and GIST
                           file folders are present.

# read csv table with above necessary data

galdat = pd.read_csv('BatchConfigInfo.csv') # Sample name for csv
                                 file with galaxy-specific data.
galdat = galdat.reset_index() #indexes pair with rows
print(galdat)

# Create a ConfigFile

SampleConfig = 'configFiles/MasterConfigTemp' #MasterConfigTemp is
                                 the MasterConfig template file
sc= open(SampleConfig, 'r')
template = sc.read() #template file to ovewrite

for index, row in galdat.iterrows():
    # replace the necessary variables
```

```
    new = template.replace('AAAA',str(row['RUN_ID'])).replace('BBBB'
                                        ,str(row['INPUT']))\
        .replace('CCCC', str(row['REDSHIFT'])).replace('DDDD', str(
                                            row['SIGMA'])).replace('
                                            EEEE', str(row['MC']))
    # Export new file
    f = open('configFiles/MasterConfig_'+str(row['RUN_ID']), 'w+')
    f.write(new)
    print('MasterConfig_'+str(row['RUN_ID']), 'was successfuly
                                        created')
    mainname = 'MasterConfig_'+str(row['RUN_ID'])

    os.system(cd)
    os.system('gistPipeline --config configFiles/MasterConfig_' +
                                        str(row['RUN_ID']) + ' --
                                        default-dir configFiles/
                                        defaultDir')
```

Code Listing B.3: Iterative extraction of σ to better constrain the pPXF initial guess. This code is written in python 3 and has been tested for compatibility for versions 3.6 and above.

```
from astropy.io import fits
import numpy as np
import pandas as pd
import os

'''

Context for the code : the following are the replaced sections of
                                    the template configuration file
                                    with their provided value
```

```
'AAAA' = 'RUN_ID'
'BBBB' ='INPUT'
'CCCC' = 'REDSHIFT'
'DDDD' = 'SIGMA'
'EEEE' = 'MC'

'''

# shell comands

cd = 'Enter Directory with .csv table. Leave Template MasterConfig
                                    inside the designated configFiles
                                    folder' #choose directory

# read csv table with above necessary data

galdat = pd.read_csv('BatchConfigInfo.csv') # name of csv table with
                                     data specific to the galaxy
                                    analyzed
galdat = galdat.reset_index() #indexes pair with rows
print(galdat)

# Create a ConfigFile

SampleConfig = 'configFiles/MasterConfigTemp' #M asterConfigTemp is
                                    name of template MasterConfig
sc= open(SampleConfig, 'r')
template = sc.read() #template file to ovewrite

for index, row in galdat.iterrows():
    # replace the necessary variables
    new = template.replace('AAAA',str(row['RUN_ID'])).replace('BBBB'
                                        ,str(row['INPUT']))\
```

```
    .replace('CCCC', str(row['REDSHIFT'])).replace('DDDD', str(
                                        row['SIGMA'])).replace('
                                        EEEE', str(row['MC']))
# Export new file
f = open('configFiles/MasterConfig_'+str(row['RUN_ID']), 'w+')
f.write(new)
print('MasterConfig_'+str(row['RUN_ID']), 'was successfuly
                                    created')
mainname = 'MasterConfig_'+str(row['RUN_ID'])

os.system(cd)
os.system('gistPipeline --config configFiles/MasterConfig_' +
                                    str(row['RUN_ID']) + ' --
                                    default-dir configFiles/
                                    defaultDir')

# extract average sigma value from previous run and run again
                                    with such value - iterate 3
                                    times
for i in range(2):
    k = 'results/' + str(row['RUN_ID']) + '/' +str(row['RUN_ID']
                                        ) +'_kin.fits'
    if i < 2:
        hdu_k = fits.open(k)
        data = hdu_k[1].data
        sigma_data = data['SIGMA']
        medsig = np.median(sigma_data)
        print('Median Sig for iteration ' + str(i+1) + ':',
                                        medsig)
        new2 = template.replace('AAAA',str(row['RUN_ID']) +'
                                        _iter_' + str(i+1)).
                                        replace('BBBB',str(row
                                        ['INPUT'])).replace('
```

```
                                        CCCC', str(row['
                                        REDSHIFT'])).replace('
                                        DDDD', str(medsig)).
                                        replace('EEEE', '0')

        filename = 'MasterConfig_' + str(row['RUN_ID']) + '
                                        _iter_' + str(i+1)
        kinname = str(row['RUN_ID'])+ '_iter_' + str(i+1) +'_kin
                                        .fits'

        f2 = open('configFiles/' + filename,'w+')
        f2.write(new2)

        os.system(cd)
        os.system('gistPipeline --config configFiles/' +
                                        filename + ' --default
                                        -dir configFiles/
                                        defaultDir')
        k = 'results/' + str(row['RUN_ID']) + '/' + kinname
    else:
        k = 'results/' + str(row['RUN_ID']) + '_iter_' + str(i)
                                        + '/' + str(row['
                                        RUN_ID']) + '_iter_' +
                                         str(i) + '_kin.fits'
        hdu_k = fits.open(k)
        data = hdu_k[1].data
        sigma_data = data['SIGMA']
        medsig = np.median(sigma_data)
        new3 = template.replace('AAAA',str(row['RUN_ID'])+'
                                        _final_iter')\
            .replace('BBBB',str(row['INPUT']))\
            .replace('CCCC', str(row['REDSHIFT']))\
            .replace('DDDD', str(medsig))\
```

```
                .replace('EEEE', '100')

            filename = 'MasterConfig_'+str(row['RUN_ID'])+'
                                                _final_iter'
            f3 = open('configFiles/'+ filename, 'w+')
            f3.write(new3)

            os.system(cd)
            os.system('gistPipeline --config configFiles/' +
                                                filename + ' --default
                                                -dir configFiles/
                                                defaultDir')
            print("median SIGMA value used for final run:",  medsig)
```

Code Listing B.4: Code inspired on the GIST mapping routine to match and extract each bin kinematics. It also contains the possibility of extracting bins at a desired radius and the plotting of σ this radius. This mapping portion of the code is currently under construction.

```
import astropy.io.fits as fits
import pandas as pd
import numpy as np


'''
This code has the purpose of extracting the velocity dispersion (
                                    sigma) for specific BinID's inside
                                     a specified radius from the
                                    center.
The SAURON data cubes have the galaxy centered at 0,0 but to make
                                    sure of this, the code searches
                                    for the BINID with the highest
```

```
                                    flux
signal and defines as such the center.

The first section uses code from the kinematic plotting portion of
                                    GIST to match the contents in the
                                    _table.fits file with the contents
of _kin.fits. The second section focuses on extracting sigma values
                                    for data within a certain radius.
                                    Finally there is a visualization
portion that uses the pixelsize determined in the _table.fits file
                                    to map the selected bins as pixels
                                     rather than points.

'''

'''
SECTION 1:

'''
PATH = 'Define the path to your GIST results folder here.'
RUN_ID = 'Insert RUN_ID here'

# open table with BIN_ID and associated data

table_hdu = fits.open(PATH + '/' + RUN_ID + '_table.fits')

idx_inside  = np.where( table_hdu[1].data.BIN_ID >= 0        )[0]

flux        = np.array( table_hdu[1].data.FLUX[idx_inside]   ) #
                                    chooses where BIN_ID > 0
snr         = np.array( table_hdu[1].data.SNR[idx_inside] )
binNum_long = np.array( table_hdu[1].data.BIN_ID[idx_inside] ) #
                                    BIN_ID where BIN_ID > 0
```

```
xbin        = np.array( table_hdu[1].data.XBIN[idx_inside] )
ybin        = np.array( table_hdu[1].data.YBIN[idx_inside] )
ubins       = np.unique( np.abs( np.array( table_hdu[1].data.BIN_ID
                                    ) ) ) # all the absolute values of
                                     the BIN_ID's that are unique
pixelsize   = table_hdu[0].header['PIXSIZE']

# open FITS file with kinematic results
hdu = fits.open(PATH + '/' + RUN_ID + '_kin.fits')

# initialize result array
result = np.zeros((len(ubins), 4))
result[:, 0] = np.array(hdu[1].data.V)
result[:, 1] = np.array(hdu[1].data.SIGMA)
result[:, 2] = np.array(hdu[1].data.ERR_SIGMA) # Only available if
                                    MC simulations are set to at least
                                     1
result[:, 3] = np.array(hdu[1].data.FORM_ERR_SIGMA)

# convert results to long version
result_long = np.zeros((len(binNum_long), result.shape[1]))
result_long[:, :] = np.nan

for i in range(len(ubins)):
    idx = np.where(ubins[i] == np.abs(binNum_long))[0]
    result_long[idx, :] = result[i, :]

result = result_long

# subtract median V value from V column so as to normalize data --
                                    can be activated if desired. Since
                                     the current focus of the code is
                                    SIGMA it is not activated.
```

```
result[:, 0] = result[:, 0] - np.nanmedian(result[:, 0])

# create new table with BIN_ID, FLUX, SNR, XBIN, YBIN, V, and SIGMA
                                    columns -- It is important to note
                                     that a run with no MC simulations
                                     will not create an ERR_SIGMA
                                    column.

data = {'BIN_ID': binNum_long,'FLUX': flux, 'SNR': snr, 'XBIN' :
                                    xbin, 'YBIN' : ybin, 'V': result[:
                                    , 0], 'SIGMA': result[:, 1], '
                                    ERR_SIGMA': result[:, 2], '
                                    FORM_ERR_SIGMA': result[:, 3]}
arr_dat = pd.DataFrame(data)

'''
SECTION 2:

This next section goes through our combined data file and selects
                                    the values of sigma within a
                                    certain radius and
allocates the row data to a new df.


        If already created, then no need to use the following
                                            function:
'''
arr_dat.to_csv(PATH + '/' + RUN_ID + '_combined.csv')

'''
        It is an extra step that helps correct the endianess.
'''
```

```
arr_dat = pd.read_csv(PATH + '/' + RUN_ID + '_combined.csv')

# Define the origin of the galaxy as the point of max flux

max_flux_index = arr_dat['FLUX'].idxmax()
max_xbin = arr_dat.loc[max_flux_index, 'XBIN']
max_ybin = arr_dat.loc[max_flux_index, 'YBIN']

# Define the radial distance
distance = ((arr_dat['XBIN'] - max_xbin) ** 2 + (arr_dat['YBIN'] -
                                    max_ybin) ** 2) ** 0.5

# Choose data with distance within our determined radius

radius = 2.24 # radius range
selected_rows = arr_dat.loc[distance <= radius]

final_selec = selected_rows[['BIN_ID', 'FLUX', 'SNR', 'XBIN', 'YBIN'
                                    , 'SIGMA','ERR_SIGMA','
                                    FORM_ERR_SIGMA']]
final_selec.to_csv(PATH + 'INSERT HERE the desired name of the table
                                     followed by .csv')

'''

SECTION 3:

This is the plotting portion of the code which will use the selected
                                    radius.
It can also be implemented on section one to obtain full SIGMA plot.

'''
```

```
import matplotlib.pyplot as plt
from scipy.interpolate import griddata

# Define grid
xgrid = np.arange(final_selec['XBIN'].min(), final_selec['XBIN'].max
                                    () + pixelsize, pixelsize)
ygrid = np.arange(final_selec['YBIN'].min(), final_selec['YBIN'].max
                                    () + pixelsize, pixelsize)
X, Y = np.meshgrid(xgrid, ygrid)

# Interpolate sigma values onto grid
Z = griddata((final_selec['XBIN'], final_selec['YBIN']), final_selec
                                    ['SIGMA'], (X, Y), method='nearest
                                    ')
Z[Z==np.nan] = np.nan

# Plot color map
plt.imshow(Z, cmap='jet', origin='lower', extent=[xgrid.min(), xgrid
                                    .max(), ygrid.min(), ygrid.max()])
plt.colorbar(label=r'$\sigma$ (km/s)')
plt.xlabel('X (arcsec)')
plt.ylabel('Y (arcsec)')
plt.show()
```

Appendix C

MasterConfig

The following text presents the presets for the template MasterConfig commands used in the batch processing and iterative codes. It is an adapted version of the MasterConfig provided by Bittner (2021). It must not be used as-is but rather be modified directly on the sample MasterConfig in found in the GIST website as it is space and position sensitive. It is, however, in the style of the original file.

```
GENERAL
| READ_DATA
| SPATIAL_MASKING
| SPATIAL_BINNING
| PREPARE_SPECTRA
| PREPARE_TEMPLATES
| KIN
| GAS
| SFH
| LS
RUN_ID  INPUT  OUTPUT   REDSHIFT   PARALLEL NCPU  LSF_DATA   LSF_TEMP
OW_CONFIG  OW_OUTPUT
```

```
| METHOD    DEBUG    ORIGIN LMIN_TOT  LMAX_TOT  LMIN_SNR  LMAX_SNR
| METHOD  MIN_SNR  MASK
| METHOD  TARGET_SNR  COVARIANCE
| METHOD  VELSCALE
| METHOD  LIBRARY  NORM_TEMP
| METHOD  SPEC_MASK  LMIN   LMAX   SIGMA   MOM   ADEG   MDEG
REDDENING   MC_PPXF
| METHOD  LEVEL   LMIN  LMAX  ERRORS   REDDENING  EBmV  EMI_FILE
| METHOD  LMIN   LMAX  SPEC_MASK     MOM  MDEG   REGUL_ERR   NOISE
FIXED
| METHOD  TYPE  LS_FILE   CONV_COR  SPP_FILE   MC_LS   NWALKER   NCHAIN

#--------------------------------------

AAAA   BBBB   .        CCCC   True       4      lsf_MUSE-WFM
lsf_MILES  False      False
| SAURON_LR  False   0,0    4800      5300      5071.5      5075.5
| default  20.      False
| voronoi  60.         0.00
| default 105
| miles    MILES/   LIGHT
| ppxf    specMask_KIN  4824.6   5281.1   DDDD     4     8      0
None        EEEE
| False  BIN     4800   5500   0        0.1,0.1    None
emissionLines.config
| False     4800   5500  specMask_SFH  4    4     1.    1.
True
```

```
| False  SPP   lsBands.config  8.4       MILES_KB_LIS8.4.fits
30      10        100


#-------------------------------------
```

Bibliography

Adam, G., Bacon, R., Courtes, G., et al. 1989, , 208, L15

Bacon, R., Adam, G., Baranne, A., et al. 1995, , 113, 347

Bacon, R., Copin, Y., Monnet, G., et al. 2001, , 326, 23, doi: 10.1046/j.1365-8711.2001.04612.x

Bahcall, J. N., Kozlovsky, B.-Z., & Salpeter, E. E. 1972, , 171, 467, doi: 10.1086/151300

Batiste, M., Bentz, M. C., Manne-Nicholas, E. R., Onken, C. A., & Bershady, M. A. 2017a, , 835, 271, doi: 10.3847/1538-4357/835/2/271

Batiste, M., Bentz, M. C., Raimundo, S. I., Vestergaard, M., & Onken, C. A. 2017b, , 838, L10, doi: 10.3847/2041-8213/aa6571

Bellovary, J. M., Holley-Bockelmann, K., Gültekin, K., et al. 2014, , 445, 2667, doi: 10.1093/mnras/stu1958

Bentz, M. C., Horenstein, D., Bazhaw, C., et al. 2014, , 796, 8, doi: 10.1088/0004-637X/796/1/8

Beuzit, J. L., Vigan, A., Mouillet, D., et al. 2019, , 631, A155, doi: 10.1051/0004-6361/201935251

Billard, F., Sharma, R., Hertz, E., Faucher, O., & Béjot, P. 2022, arXiv e-prints, arXiv:2201.10417, doi: 10.48550/arXiv.2201.10417

Bittner, A. 2021, in Extragalactic Spectroscopic Surveys: Past, Present and Future of Galaxy Evolution (GALSPEC2021), 2, doi: 10.5281/zenodo.4721502

Blandford, R. D., & McKee, C. F. 1982a, , 255, 419, doi: 10.1086/159843

—. 1982b, , 255, 419, doi: 10.1086/159843

Bundy, K., Bershady, M. A., Law, D. R., et al. 2015, , 798, 7, doi: 10.1088/0004-637X/798/1/7

Cappellari, M. 2017, , 466, 798, doi: 10.1093/mnras/stw3020

—. 2022, arXiv e-prints, arXiv:2208.14974, doi: 10.48550/arXiv.2208.14974

Cappellari, M., & Copin, Y. 2003, , 342, 345, doi: 10.1046/j.1365-8711.2003.06541.x

Cappellari, M., & Emsellem, E. 2004, , 116, 138, doi: 10.1086/381875

Cappellari, M., Emsellem, E., Krajnović, D., et al. 2011, , 413, 813, doi: 10.1111/j.1365-2966.2010.18174.x

Cappellari, M., Scott, N., Alatalo, K., et al. 2013a, , 432, 1709, doi: 10.1093/mnras/stt562

—. 2013b, , 432, 1709, doi: 10.1093/mnras/stt562

Cid Fernandes, R. 2018, , 480, 4480, doi: 10.1093/mnras/sty2012

Closs, M. F., Ferruit, P., Lobb, D. R., et al. 2008, in Society of Photo-Optical Instrumentation Engineers (SPIE) Conference Series, Vol. 7010, Space Telescopes and Instrumentation 2008: Optical, Infrared, and Millimeter, ed. J. Oschmann,

Jacobus M., M. W. M. de Graauw, & H. A. MacEwen, 701011, doi: 10.1117/12.788820

Davis, B. L., Graham, A. W., & Cameron, E. 2019, , 873, 85, doi: 10.3847/1538-4357/aaf3b8

Davis, B. L., Graham, A. W., & Seigar, M. S. 2017, , 471, 2187, doi: 10.1093/mnras/stx1794

de Zeeuw, P. T., Bureau, M., Emsellem, E., et al. 2002, , 329, 513, doi: 10.1046/j.1365-8711.2002.05059.x

Dressler, A. 1989, in Active Galactic Nuclei, ed. D. E. Osterbrock & J. S. Miller, Vol. 134, 217

Dressler, A., & Richstone, D. O. 1988, , 324, 701, doi: 10.1086/165930

Emsellem, E., Cappellari, M., Peletier, R. F., et al. 2004, , 352, 721, doi: 10.1111/j.1365-2966.2004.07948.x

Enard, D., Lund, G., & Tarenghi, M. 1983, The Messenger, 33, 32

Event Horizon Telescope Collaboration, Akiyama, K., Alberdi, A., et al. 2019, , 875, L1, doi: 10.3847/2041-8213/ab0ec7

Falcón-Barroso, J., Bacon, R., Bureau, M., et al. 2006, , 369, 529, doi: 10.1111/j.1365-2966.2006.10261.x

Ferrarese, L., & Merritt, D. 2000, , 539, L9, doi: 10.1086/312838

Gebhardt, K., Bender, R., Bower, G., et al. 2000, , 539, L13, doi: 10.1086/312840

Genzel, R., Förster Schreiber, N. M., Übler, H., et al. 2017, , 543, 397, doi: 10.1038/nature21685

Gould, A. 2013, arXiv e-prints, arXiv:1303.0834, doi: 10.48550/arXiv.1303.0834

Gültekin, K., Richstone, D. O., Gebhardt, K., et al. 2011, , 741, 38, doi: 10.1088/0004-637X/741/1/38

Hill, L., Thomas, D., Maraston, C., et al. 2022, , 517, 4275, doi: 10.1093/mnras/stac2992

Hoyle, F., & Fowler, W. A. 1963, , 125, 169, doi: 10.1093/mnras/125.2.169

Hu, J. 2008, , 386, 2242, doi: 10.1111/j.1365-2966.2008.13195.x

Keel, W. C. 1996, , 111, 696, doi: 10.1086/117816

Kenworthy, M. A. 1998, PhD thesis, University of Cambridge, UK

Kleinmann, S. G. 1992, in Astronomical Society of the Pacific Conference Series, Vol. 103, Robotic Telescopes in the 1990s, ed. A. V. Filippenko, 203–212

Kormendy, J. 1993, in Galactic Bulges, ed. H. Dejonghe & H. J. Habing, Vol. 153, 209

Kormendy, J., & Ho, L. C. 2013, arXiv e-prints, arXiv:1308.6483, doi: 10.48550/arXiv.1308.6483

Kuntschner, H., Emsellem, E., Bacon, R., et al. 2006, , 369, 497, doi: 10.1111/j.1365-2966.2006.10153.x

Lynden-Bell, D. 1969, , 223, 690, doi: 10.1038/223690a0

—. 1978, , 17, 185, doi: 10.1088/0031-8949/17/3/009

Lynden-Bell, D., & Rees, M. J. 1971, , 152, 461, doi: 10.1093/mnras/152.4.461

Magorrian, J., Tremaine, S., Richstone, D., et al. 1998, , 115, 2285, doi: 10.1086/300353

Marconi, A., & Hunt, L. K. 2003, , 589, L21, doi: 10.1086/375804

Martín-Navarro, I., Vazdekis, A., Falcón-Barroso, J., et al. 2018, , 475, 3700, doi: 10.1093/mnras/stx3346

Merrell, K. A., Vasiliev, E., Bentz, M. C., Valluri, M., & Onken, C. A. 2022, arXiv e-prints, arXiv:2212.02484, doi: 10.48550/arXiv.2212.02484

Nowak, N., Thomas, J., Erwin, P., et al. 2010, , 403, 646, doi: 10.1111/j.1365-2966.2009.16167.x

Onken, C. A., Ferrarese, L., Merritt, D., et al. 2004, , 615, 645, doi: 10.1086/424655

Pacucci, F., Loeb, A., Mezcua, M., & Martín-Navarro, I. 2018, , 864, L6, doi: 10.3847/2041-8213/aad8b2

Poggianti, B. M., Jaffé, Y. L., Moretti, A., et al. 2017, , 548, 304, doi: 10.1038/nature23462

Richstone, D., Bower, G., & Dressler, A. 1990, , 353, 118, doi: 10.1086/168596

Roy, N., Bundy, K., Nevin, R., et al. 2021, , 913, 33, doi: 10.3847/1538-4357/abf1e6

Salpeter, E. E. 1964, , 140, 796, doi: 10.1086/147973

Sánchez, S. F., Kennicutt, R. C., Gil de Paz, A., et al. 2011, in Highlights of Spanish Astrophysics VI, ed. M. R. Zapatero Osorio, J. Gorgas, J. Maíz Apellániz, J. R. Pardo, & A. Gil de Paz, 339–344, doi: 10.48550/arXiv.1012.3002

Sarzi, M., Rix, H.-W., Shields, J. C., et al. 2001, , 550, 65, doi: 10.1086/319724

Sarzi, M., Falcón-Barroso, J., Davies, R. L., et al. 2006, , 366, 1151, doi: 10.1111/j.1365-2966.2005.09839.x

Schmidt, M. 1963, , 197, 1040, doi: 10.1038/1971040a0

Shankar, F., Bernardi, M., Sheth, R. K., et al. 2016, , 460, 3119, doi: 10.1093/mnras/stw678

Valluri, M., Merritt, D., & Emsellem, E. 2004, , 602, 66, doi: 10.1086/380896

van der Marel, R. P., Cretton, N., de Zeeuw, P. T., & Rix, H.-W. 1998, , 493, 613, doi: 10.1086/305147

Vazdekis, A., Sánchez-Blázquez, P., Falcón-Barroso, J., et al. 2010, , 404, 1639, doi: 10.1111/j.1365-2966.2010.16407.x

Verolme, E. K., Cappellari, M., van de Ven, G., et al. 2003, in Galaxies and Chaos, ed. G. Contopoulos & N. Voglis, Vol. 626, 279–285, doi: 10.1007/978-3-540-45040-5_22

Zel'dovich, Y. B. 1964, Soviet Physics Doklady, 9, 195